Chapter 2
Two-Particle Systems Under Conditions of Sonic Vacuum

In this section, we investigate resonance energy transport in a purely nonlinear system, wherein harmonic oscillations are prohibited by the properties of the system potential of degree higher than two. So, in contrast to the models considered in the previous sections, the potential of this system does not contain quadratic terms. Hence, the system does not exhibit the quasi-linear behavior; furthermore, there is no constant natural frequencies predetermining resonance properties of the system in the quasi-linear approximation. This implies that the study of resonance processes and resonance energy transport in a purely nonlinear system requires a special approach.

The basic model considered in this section comprises two weakly coupled purely nonlinear oscillators, wherein initial energy is imported to one of them. Numerical simulations reveal the existence of strong classical beat oscillations corresponding to complete recurrent resonant energy exchanges between the oscillators in the state of sonic vacuum, where no resonance frequencies can be defined. In this study, we show that both intense energy exchange and transition to energy localization are adequately described in the framework of the LPT concept. We show that the occurrence of the recurrent energy exchanges in this highly degenerate model strictly depends on the system parameters. For instance, choosing the parameter of coupling below a certain threshold leads to the significant energy localization on one of the oscillators; on the contrary, increasing the strength of coupling above the threshold brings to the formation of a strong beating response.

Analytical studies pursued in this section predict the occurrence of the strong beating phenomenon and provide necessary conditions for its emergence. Moreover, a careful analysis of the beating phenomenon reveals a qualitatively new global bifurcation of highly non-stationary regime.

Two systems considered in this chapter are similar to a weightless unstretched preliminarily string with two symmetrically located point-like masses. In the first model (Sect. 2.1), we restrict the motion by transversal (to the string) direction only (scalar case). In Sect. 2.2, this restriction is removed.

L.I. Manevitch et al., *Nonstationary Resonant Dynamics of Oscillatory Chains and Nanostructures*, Foundations of Engineering Mechanics,
DOI 10.1007/978-981-10-4666-7_2

2.1 Weakly Coupled Oscillators Under Conditions of Local Sonic Vacuum

If the motion of the particles is transversal to the weightless string itself, the coupling between the particles is realized by the local strongly nonlinear interactions. If the preliminary stretching of the string is absent, they are cubic functions in the main approximation. However, we consider even more general case when the power may be not only three but an arbitrary odd integer.

2.1.1 Evidence of Energy Localization and Exchange in Coupled Oscillators in the State of Sonic Vacuum

We study energy localization and complete recurrent energy transport in a homogeneous system of two coupled anharmonic oscillators in the state of sonic vacuum. This model (in the case of cubic inter-particle interaction) is mathematically equivalent to weightless string with two symmetrically located identical particles if a preliminary stretching is absent and the motion occurs in the transversal direction only. The main goal is to describe the transition from initial energy localization on a single oscillator to complete recurrent energy exchanges (strong beating phenomenon) between the oscillators due to variations of the system parameters

The model under consideration comprises two identical anharmonic oscillators coupled with an anharmonic spring. The non-dimensional equations of motion are given by

$$\begin{aligned} \frac{\mathrm{d}^2 x_1}{\mathrm{dt}^2} + x_1^n &= \chi(x_2 - x_1)^n, \\ \frac{\mathrm{d}^2 x_2}{\mathrm{dt}^2} + x_2^n &= \chi(x_1 - x_2)^n. \end{aligned} \tag{2.1}$$

here $n = 2k + 1, \quad k = 1, 2, 3, \ldots$; the parameter χ denotes coupling stiffness. Initial conditions $x_1 = X_1$, $v_1 = \mathrm{d}x_1/\mathrm{d}t = V_1$, $x_2 = 0$, $v_2 = \mathrm{d}x_2/\mathrm{d}t = 0$ at $t = 0$ correspond to complete initial localization of the system energy on the first oscillator with the second oscillator being initially at rest.

It is important to emphasize that the system (2.1) is homogeneous, and therefore, its total energy E can be normalized to unity ($E = 1$) by choosing appropriate rescaling of the dependent and independent variables. This means that the global system dynamics is energy-independent and can be studied for an arbitrary value of the total energy level.

Below, we illustrate numerically the existence of two different regimes such as energy localization on the initially excited oscillator and complete energy exchanges between the oscillators. We also show that the first regime corresponds

to the non-resonant behavior of the coupled oscillators while the second one is triggered by the formation of permanent 1:1 resonance capture resulting in the complete recurrent energy transport between the oscillators.

2.1.2 Energy Localization

Figure 2.1a depicts instantaneous energy $E_i(t) = \dot{x}_i^2/2 + (n+1)^{-1}x_i^{n+1}$ of each of the oscillators in the system with parameters $\chi = 0.12$, $n = 3$ and initial conditions $x_1 = 1$, $v_1 = 0$, $x_2 = 0$, $v_2 = 0$ at $t = 0$. Figure 2.1b, c illustrate the fast Fourier transform (FFT) transforms of $x_1(t)$ and $x_2(t)$, respectively.

In Fig. 2.1a, one can observe localization of the initial energy on the first oscillator. This result is not surprising, as the system under consideration is purely nonlinear (sonic vacuum), and strong spatial energy localization on certain fragments of the system is expected. Moreover, fast Fourier transform (FFT) diagrams presented in Fig. 2.1b, c show that this type of response exhibits a trivial non-resonant behavior, where the amplitude of a main frequency component of the first oscillator far exceeds the amplitude of the main components of the second oscillator. Also, the second oscillator possesses two comparable components with remote frequencies exhibiting a clear subharmonic motion. The detailed analysis of this type of response is performed in Sect. 2.1.4.

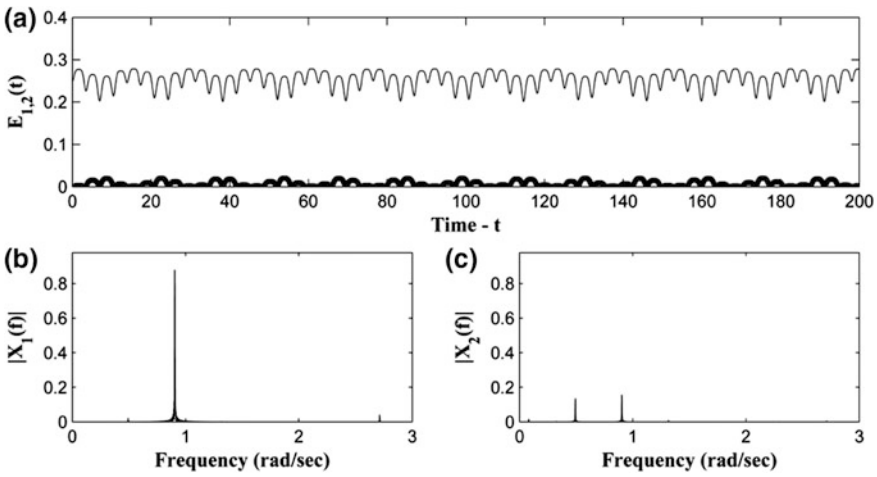

Fig. 2.1 Regime of energy localization. **a** Instantaneous energies recorded on the first and the second oscillators ($E_1(t)$ *thin solid line*, $E_2(t)$ *bold solid line*); **b** fast Fourier transform of the response of the first oscillator $x_1(t)$; **c** fast Fourier transform of the response of the second oscillator $x_2(t)$

2.1.3 *Complete Energy Exchanges (Strong Beating Response)*

Slightly increasing the coupling parameter χ, we observe a global change of the response. In particular, instead of energy localization on the first oscillator we observe the formation of a beating response characterized by complete energy exchange between the oscillators. Instantaneous energy $E_i(t) = \dot{x}_i^2/2 + (n+1)^{-1}x_i^{n+1}$ is plotted in Fig. 2.2a for each of the oscillators in the system with parameters $\chi = 0.18$, $n = 3$ and initial conditions $x_1 = 1$, $v_1 = 0$, $x_2 = 0$, $v_2 = 0$ at $t = 0$. Figure 2.2b, c illustrates the FFT transforms of $x_1(t)$ and $x_2(t)$, respectively.

Figure 2.2a depicts the beating response characterized by complete recurrent energy exchange between the oscillators. FFT diagrams in Fig. 2.2b, c reveal the resonant nature of the response ensuring the formation of 1:1 resonance between the oscillators, which, in turn, leads to the strong beating response.

It is important to note that beating oscillations are usually observed in linear or weakly nonlinear systems possessing at least one pair of close natural frequencies (Manevitch and Gendelman 2011; Manevitch and Smirnov 2010a, b, c). In these cases, the resonance frequency of the response is determined either by the natural frequency of the linear subsystem or by the frequency of a periodic excitation. However, in the system under consideration subjected to the state of acoustic vacuum the resonant frequency is determined by the energy level of initial excitation. Therefore, resonance frequencies observed in Fig. 2.2b, c are obviously amplitude-dependent. This means that an increase in the initial amplitude of the first oscillator results in an increase in the resonant frequency of oscillations.

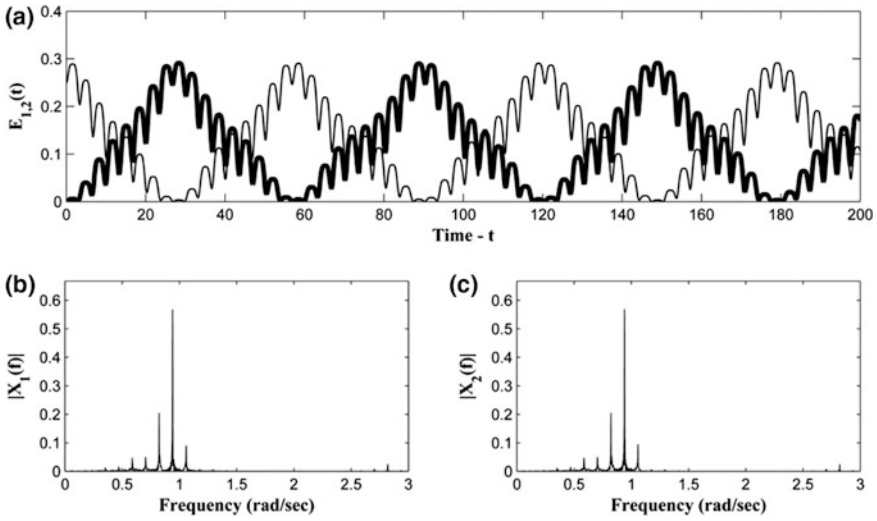

Fig. 2.2 Strong beating response. **a** Instantaneous energies recorded on the first and the second oscillators ($E_1(t)$—*thin dotted line*, $E_2(t)$—*bold solid line*); **b** FFT of $x_1(t)$; **c** FFT of $x_2(t)$

2.1.4 Asymptotic Analysis of Resonance Motion

This section suggests theoretical analysis of the near-resonant behavior of system (2.1). Special emphasis is given to an analytical description of the formation and the annihilation of a regular beating response, along with the local and global bifurcation analysis of the system dynamics.

Given the pure resonant nature of a strong beating regime, it is quite reasonable to anticipate its formation in the neighborhood of the 1:1 resonance manifold. It is well known that the phenomenon of 1:1 resonance capture provides maximum energy transfer between weakly coupled identical oscillators. Thus, in order to depict analytically the regime of complete energy transfer, as well as to find necessary conditions for its existence, it is convenient to consider the system dynamics in a neighborhood of the 1:1 resonance manifold.

Assuming resonance interactions, we rewrite (2.1) as follows:

$$\frac{\mathrm{d}^2 x_k}{\mathrm{d}t^2} + \Omega^2 x_k = \varepsilon\mu\left[\chi(x_{3-k} - x_k)^n - x_{k^n} + \Omega^2 x_k\right], \quad k = 1, 2, \tag{2.2}$$

where Ω denotes the resonance frequency depending on the system energy, ε is a small parameter of the system, $\mu = 1/\varepsilon$. As in the previous sections, we assume that the sum in the square brackets is small but the expression $\mu\left[\chi(x_{3-k} - x_k)^n - x_{k^n} + \Omega^2 x_k\right]$ is of $O(1)$ in the vicinity of resonance.

We underline that the representation of equations of motion in the form (2.2) allows us to investigate the purely nonlinear system in the framework of the quasi-linear theory and to employ the earlier developed methods. In the first step, we introduce the new complex variables as follows:

$$u_k = \frac{1}{2\imath}\left(Y_k \mathrm{e}^{i\Omega\tau_0} - Y_k^* \mathrm{e}^{-i\Omega\tau_0}\right), \quad v_k = \frac{\Omega}{2}\left(Y_k \mathrm{e}^{i\Omega\tau_0} + Y_k^* \mathrm{e}^{-i\Omega\tau_0}\right), \tag{2.3}$$

and then substitute (2.3) into (2.1) to obtain the equations for Y_k, Y_k^* with the right-hand sides of $O(\varepsilon)$ (see Starosvetsky and Ben-Meir 2013 for more details). In the next step, the complex amplitude $Y_k(t, \varepsilon)$ is sought in the form of the expansion $Y_k(t, \varepsilon) = \varphi_k^{(0)}(\tau_1) + \varepsilon\, \varphi_k^{(1)}(t, \tau_1) + \varepsilon^2 \ldots$, with the slow main term $\varphi_k^{(0)}(\tau_1)$, where $\tau_1 = \varepsilon t$ is the leading-order slow timescale. Then, applying the multiple scales methodology, we derive the following equation for the leading-order slow amplitudes $\varphi_k^{(0)}(\tau_1)$ (detailed arguments are provided in Starosvetsky and Ben-Meir 2013):

$$\frac{\mathrm{d}\varphi_k^{(0)}}{\mathrm{d}\tau_1} = i\mu\left(\frac{C^n_{(n-1)/2}}{(2\Omega)^n}\left|\varphi_k^{(0)}\right|^{n-1}\varphi_k^{(0)} - \frac{\Omega}{2}\varphi_k + \chi\frac{C^n_{(n-1)/2}}{(2\Omega)^n}\left|\varphi_{3-k}^{(0)} - \varphi_k^{(0)}\right|^{n-1}\left(\varphi_{3-k}^{(0)} - \varphi_k^{(0)}\right)\right)$$
$$k = 1, 2 \tag{2.4}$$

where $C^n_{(n-1)/2}$ is the binomial coefficient. It is easy to conclude that system (2.4) possesses two integrals of motion

$$\begin{aligned} N^2 &= \left|\varphi_1^{(0)}\right|^2 + \left|\varphi_2^{(0)}\right|^2 \\ H &= \left|\phi_1^{(0)}\right|^{(n+1)} + \left|\phi_2^{(0)}\right|^{(n+1)} + \mu^*\left|\phi_1^{(0)} - \phi_2^{(0)}\right|^{(n+1)}. \end{aligned} \tag{2.5}$$

The first integral of motion allows for a convenient change of coordinates

$$\varphi_1^{(0)} = N\,\cos\theta e^{i\delta_1}, \quad \varphi_2^{(0)} = N\,\sin\theta e^{i\delta_2}. \tag{2.6}$$

Substituting (2.6) into (2.4), considering the relative phase $\delta = \delta_1 - \delta_2$ as a new variable, and rescaling the independent variable by law $\tau = \left[C^n_{(n-1)/2}N^{n-1}/(2\Omega)^n\right]\tau_1$, we reduce (2.4) to the real-valued system

$$\begin{aligned} \frac{\mathrm{d}\delta}{\mathrm{d}\tau} &= \mu\left[\cos^{n-1}\theta - \sin^{n-1}\theta + 2\chi(1-\sin 2\theta\,\cos\delta)^{\frac{n-1}{2}}\cot 2\theta\,\cos\delta\right], \\ \frac{\mathrm{d}\theta}{\mathrm{d}\tau} &= \mu\chi(1-\sin 2\theta\,\cos\delta)^{\frac{n-1}{2}}\sin\,\delta. \end{aligned} \tag{2.7}$$

It is important to note that system (2.7) does not involve the energy-dependent frequency Ω and governed only by the constant parameters χ and n, thus making the global dynamics of system (2.7) invariant to the slow amplitudes $\left|\varphi_1^{(0)}\right|, \left|\varphi_2^{(0)}\right|$. We will show that variations of the governing parameters χ and n lead to both local and global bifurcations.

2.1.5 *Fixed Points and NNMs in the Neighborhood of Resonance*

The further study of the system dynamics is concentrated on the analysis of system (2.7). First, we find fixed points of (2.7). By setting $\mathrm{d}\theta/\mathrm{d}\tau = \mathrm{d}\delta/\mathrm{d}\tau = 0$, we obtain the following algebraic equations defining the fixed points of (2.7):

$$\begin{aligned} &\cos^{n-1}\theta - \sin^{n-1}\theta + 2\chi(1-\sin 2\theta\,\cos\delta)^{\frac{n-1}{2}}\cot 2\theta\,\cos\delta = 0, \\ &(1-\sin 2\theta\,\cos\delta)^{\frac{n-1}{2}}\sin\delta = 0. \end{aligned} \tag{2.8}$$

By setting $\cos 2\theta = 0$, $\sin\,\delta = 0$, we obtain the following set of fixed points:

$$\begin{aligned} &\left(\delta_1^{(1)}, \theta_1^{(1)}\right) = (0, \pi/4); \left(\delta_2^{(1)}, \theta_2^{(1)}\right) = (\pi, 3\pi/4); \\ &(\delta_1^{(2)}, \theta_1^{(2)}) = (0, 3\pi/4); (\delta_2^{(2)}, \theta_2^{(2)}) = (\pi, \pi/4). \end{aligned} \tag{2.9}$$

The first pair of fixed points corresponds to the in-phase nonlinear normal mode (NNM) of the original system (2.1), while the second one corresponds to the out-of-phase NNM.

Additional fixed points $(\delta_k^{(3)}, \theta_k^{(3)})$, $k = 1, 2$, are defined by the conditions $\cos 2\theta \neq 0$, $\sin \delta = 0$, that is,

$$\left(\cos^{n-1}\theta - \sin^{n-1}\theta\right)\tan 2\theta - 2\chi(1 + \sin 2\theta)^{\frac{n-1}{2}} = 0, \quad \delta = \pi, \tag{2.10}$$

$$\left(\cos^{n-1}\theta - \sin^{n-1}\theta\right)\tan 2\theta + 2\chi(1 - \sin 2\theta)^{\frac{n-1}{2}} = 0, \quad \delta = 0. \tag{2.11}$$

As mentioned above, the global system dynamics is governed by the parameters χ and n. In Fig. 2.3, we plot the solutions of Eq. (2.10) corresponding to $\delta = \pi$ versus variations of the parameter χ for four different values of n. It is easy to see that the branches of solutions bifurcate from the point $(\pi, \pi/4)$. We will not illustrate solutions of (2.11) because they are similar to those of (2.10) but for the range of $\theta \in [\pi, 2\pi]$.

Figure 2.3 demonstrates a qualitative change of the solutions of (2.10) for $n > 5$. These topological changes represent the results of transition from a supercritical to a subcritical pitchfork bifurcation undergone by the fixed points described in (Zhupiev and Mikhlin 1981, 1984). Note that the appearance of the subcritical bifurcation of the fixed points has a significant effect on the occurrence of strong beats as well as on the shape of the response.

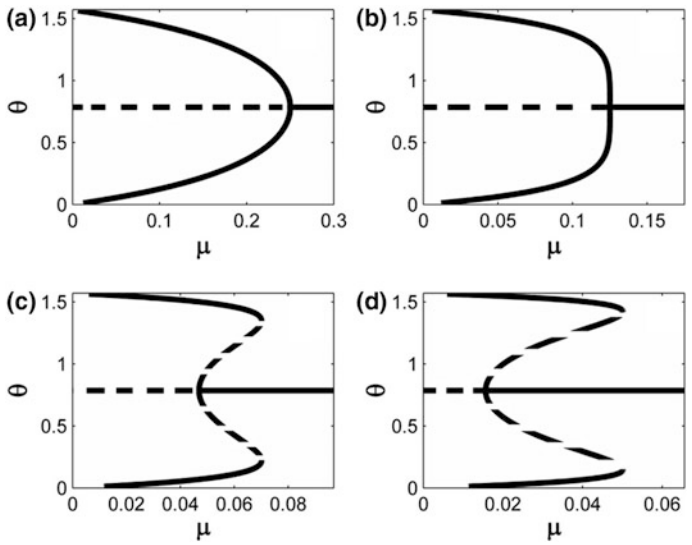

Fig. 2.3 Solutions of (2.10) versus variation of coupling strength χ: **a** $n = 3$; **b** $n = 5$; **c** $n = 5$; **d** $n = 9$. Stable branches of solution are denoted by *bold solid lines*, unstable branches of solutions are denoted by *dashed lines*. Horizontal axes $\theta = \pi/4$ correspond to the fixed point $\theta_2^{(2)}$

Before proceeding with the analysis of strong beating response, we analytically prove the occurrence of a subcritical pitchfork bifurcation at $n > 5$. In the first step, one can deduce that the branches of the solutions of (2.10) bifurcate from the fixed point $\theta_2^{(2)} = \pi/4$. To analyze motion near $\theta = \pi/4$, Eq. (2.10) is rewritten as

$$\chi = \frac{\left(\cos^{n-1}\theta - \sin^{n-1}\theta\right)\tan 2\theta}{2(1+\sin 2\theta)^{\frac{n-1}{2}}}. \tag{2.12}$$

It follows from (2.12) that $\lim_{\theta\to\pi/4}(\partial\chi/\partial\theta) = 0$. In the next step, we insert the expansion $\theta = \pi/4 + \tilde{\theta}$, ($|\tilde{\theta}| \ll 1$) into (2.12) to obtain

$$\chi = \frac{n-1}{2^n} + \frac{n(n-1)(n-2)}{3(2)^{n+1}}\tilde{\theta}^2 + O\left(\tilde{\theta}^3\right). \tag{2.13}$$

The first term in the right-hand side of (2.13) represents the first bifurcation value of coupling strength χ

$$\chi_{cr}^{(1)} = 2^{-n}(n-1), \tag{2.14}$$

at which the fixed point $(\delta_2^{(2)}, \theta_2^{(2)}) = (\pi, \pi/4)$ is transformed from the saddle point to the stable center for an arbitrary value of n. The transformation of the saddle point can be easily proved by performing a linear stability analysis (Starosvetsky and Ben-Meir 2013).

It follows from expansion (2.13) that the coefficient of the quadratic term is always positive for $n > 5$. In the special case of $n = 5$, this coefficient equals zero. In this case, one can easily show that the coefficient of the higher-order term in the expansion (i.e., the forth-order term) is negative. Hence, expansion (2.13) proves the formation of a subcritical pitchfork bifurcation for $n > 5$.

2.1.6 *Limiting Phase Trajectories*

Figures 2.3 and 2.4 depict phase portraits of system (2.7) for $n = 3$ and $n = 7$. The choice of these values of the parameter n is not arbitrary; it aims to show the global changes in the system dynamics caused by the transition from supercritical ($n > 5$) to subcritical ($n > 5$) pitchfork bifurcations.

In terms of the model (2.7), complete energy exchanges between the oscillators are associated with the *limiting phase trajectory* (LPT), which passes through zero point $\delta = \theta = 0$ and reaches the value $\theta = \pi/2$. We underline that, unlike the previous sections, there is no way to distinguish quasi-linear, moderately nonlinear, and strongly nonlinear regimes, because the system does not exhibit the quasi-linear behavior.

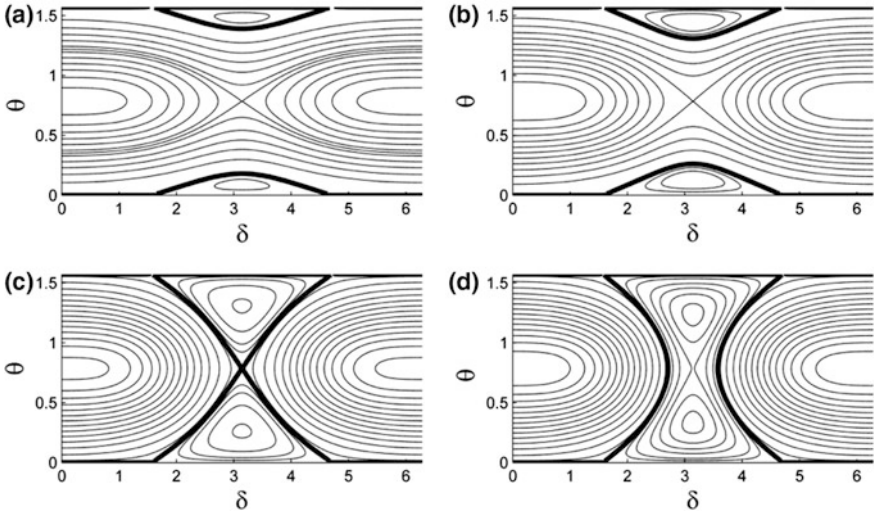

Fig. 2.4 Phase portrait of system (2.7) with $n = 3$ and different coupling strength: **a** $\chi = 0.075$, **b** $\chi = 0.1$; **c** $\chi = 0.1667$; **d** $\chi = 0.19$. Limiting phase trajectories (LPTs) are denoted by *bold lines* on each plot

Figure 2.4a, b demonstrate special orbits (bold lines) satisfying the initial condition $\delta = \theta = 0$. However, motion along these orbits cannot lead to complete energy exchange between the oscillators, as the trajectory does not reach the value $\theta = \pi/2$. Below, we refer to this kind of the phase trajectory as the LPT of the first kind.

Increasing the value of χ up to a certain critical value $\chi_{cr}^{(2)}$, one can observe the coalescence of the LPT of the first kind with the separatrix (Fig. 2.4c). This coalescence leads to the global bifurcation resulting in the formation of an LPT of the qualitatively different type (Fig. 2.3d), that is, of the LPT of the second kind.

Phase portraits in Fig. 1.18a are qualitatively similar to that ones in Fig. 2.4a. However, slightly increasing the strength of coupling χ (Fig. 2.5b), we observe the occurrence of an additional pair of unstable fixed points, and the transition of the fixed point $(\delta_2^{(2)}, \theta_2^{(2)})$ from the saddle point to the stable center. The latter observation is a result of the above described subcritical pitchfork bifurcation. Clearly, except the regular LPT starting at $\theta = 0$, there exists an additional branch of the LPT (we will refer to it as the "LPT bubble") encircling the center $(\delta_2^{(2)}, \theta_2^{(2)})$. This new type of LPT is illustrated in Fig. 2.5c. At a certain critical value $\chi = \chi_{cr}^{(2)}$, the regular LPT collides with the "bubble" LPT exactly at the saddle point, entailing the occurrence of the LPT of the second kind (Fig. 2.5d). The newborn LPT of the second kind has a topology different from that one in the case of $n = 3$ reported in previous sections.

It is seen in Fig. 2.5 that the LPT of the second kind in the case of $n > 5$ has a near rectangular shape instead of the triangle observed at $n = 3$ and $n = 5$.

In order to derive analytical conditions of the occurrence of the LPT of the second kind for any value of n, as well as to find a critical value $\chi_{cr}^{(2)}$, we consider the second integral of motion (2.5). Expressing H in terms of (θ, δ), one obtains

$$H(\delta, \theta, \chi) = \cos^{n+1}\theta + \sin^{n+1}\theta + \chi(1 - \sin 2\theta \cos\delta)^{(n+1)/2}. \tag{2.15}$$

Equation (2.15) depicts phase trajectories of (2.7). We recall that the LPT of any kind passes through zero point $\delta = \theta = 0$. Substituting $\theta = 0$ into (2.15) yields the following exact value of $H(\delta, \theta, \chi)$ corresponding to the LPT:

$$H_{\mathrm{LPT}}(\delta, \theta, \chi) = 1 + \chi. \tag{2.16}$$

In the case of $n < 7$, an increase in the coupling parameter χ up to a critical value $\chi_{cr}^{(2)}$ corresponds to the transition from the LPT of the first kind to the LPT of the second kind. Since the LPT passes through the saddle point $(\delta_2^{(2)}, \theta_2^{(2)}) = (\pi, \pi/4)$, the value $\chi = \chi_{cr}^{(2)}$ can be found from the equality

$$H_{\mathrm{LPT}}(\pi, \pi/4, \chi_{cr}^{(2)}) = 1 + \chi_{cr}^{(2)}. \tag{2.17}$$

It follows from (2.15) and (2.17) that

$$\chi_{cr}^{(2)} = \left(1 - 2^{-\frac{(n-1)}{2}}\right)\left(2^{\frac{(n-1)}{2}} - 1\right). \tag{2.18}$$

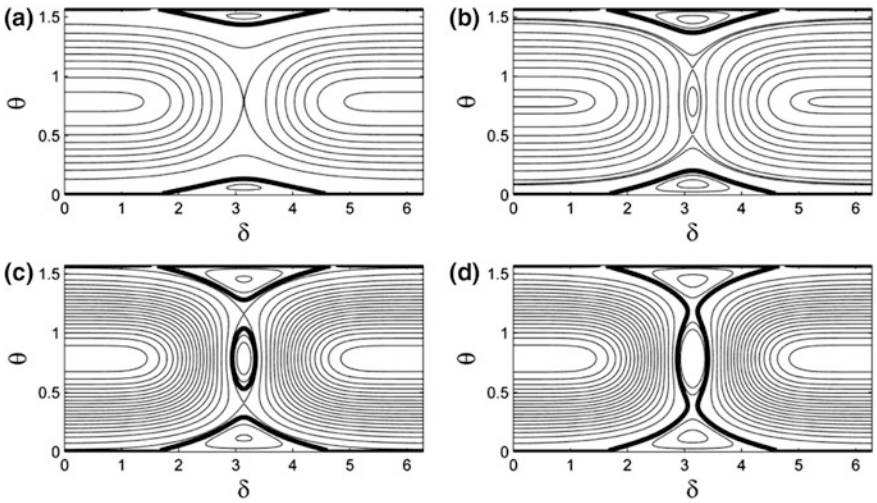

Fig. 2.5 Phase portrait of system (2.7) with $n = 7$ and different coupling strength: **a** $\chi = 0.040$; **b** $\chi = 0.055$; **c** $\chi = 0.061$; **d** $\chi = 0.063$. Limiting phase trajectories (LPTs) are denoted with the *bold line* on each plot

We recall that the critical value $\chi_{\mathrm{cr}}^{(2)}$ is associated with the transition from the LPT of the first kind to the LPT of the second kind only for $n = 3$ and $n = 5$. If $n > 5$, then, requiring the fixed point $(\delta_2^{(2)}, \theta_2^{(2)})$ to lie on the LPT, we find a critical value $\chi_{\mathrm{cr}}^{(3)}$ corresponding to the occurrence of the LPT "bubble." To this end, we require the branch of the LPT to cross a saddle point branching out from $(\delta_2^{(2)}, \theta_2^{(2)})$ through the pitchfork bifurcation. This branch of the solutions is given by Eq. (2.10). Thus, solving the following nonlinear system:

$$\begin{aligned} &\left(\cos^{n-1}\theta - \sin^{n-1}\theta\right)\tan 2\theta - 2\chi_{cr}^{(3)}(1+\sin 2\theta)^{\frac{n-1}{2}} = 0, \\ &\cos^{n+1}\theta + \sin^{n+1}\theta + \chi_{cr}^{(3)}(1+\sin 2\theta)^{\frac{n+1}{2}} = 1 + \chi_{cr}^{(3)}, \end{aligned} \tag{2.19}$$

one can derive a new criterion for the transition from localization to complete energy transfer for the case of $n > 5$. In Table 2.1, we summarize critical values of coupling strength χ corresponding to different types of dynamical transitions.

2.1.7 Numerical Analysis of the Fundamental Model

We perform numerical verifications of the theoretical model suggested in the previous section. We compare the response of the original system (2.1) with initial conditions $x_1(0) = 1$, $x_2(0) = 0$; $v_1(0) = v_2(0) = 0$ with the slow envelope (2.4) satisfying the corresponding initial conditions $\varphi_1(0) = i$, $\varphi_2(0) = 0$. To confirm the validity of the theoretical models for two different topologies of the LPT, we choose two representative values of n, namely $n = 3$ (Fig. 2.6) and $n = 7$ (Fig. 2.6).

From the results in Fig. 2.6a ($n = 3$), it is clear that the choice of coupling strength χ below the predicted threshold ($\chi < \chi_{\mathrm{cr}}^{(2)} = 0.167$) leads to energy localization on the first oscillator. However, if the value of χ is increasing above the threshold ($\chi > \chi_{\mathrm{cr}}^{(2)}$), we clearly observe the occurrence of a strong beating response, i.e., complete energy exchanges between the oscillators (Fig. 2.6b). Moreover, the slow flow envelop given by (2.4) is in a very good agreement with the full model (2.1). This means that the analytical model clearly recovers the mechanism of the transition from localization to recurrent energy transfer observed in the full model.

$$\Sigma = \{x_1 = 0, \dot{x}_1 > 0\} \cap \{E(x_1, \dot{x}_1, x_2, \dot{x}_2) = 1\}$$

Table 2.1 Critical values of coupling strength χ versus for different types of dynamical transitions

	Pitchfork bifurcation value	Formation of the LPT "bubble"	Transition from localization to a complete energy transfer
$n > 7$	$\chi_{\mathrm{cr}}^{(1)} = 2^{-n}(n-1)$	–	$\chi_{\mathrm{cr}}^{(2)} = \left(1 - 2^{-\frac{(n-1)}{2}}\right)\left(2^{\frac{(n-1)}{2}} - 1\right)$
$n > 7$	$\chi_{\mathrm{cr}}^{(1)} = 2^{-n}(n-1)$	$\chi_{\mathrm{cr}}^{(2)} = \left(1 - 2^{-\frac{(n-1)}{2}}\right)\left(2^{\frac{(n-1)}{2}} - 1\right)$	$\chi_{\mathrm{cr}}^{(3)}$-solution of (25)

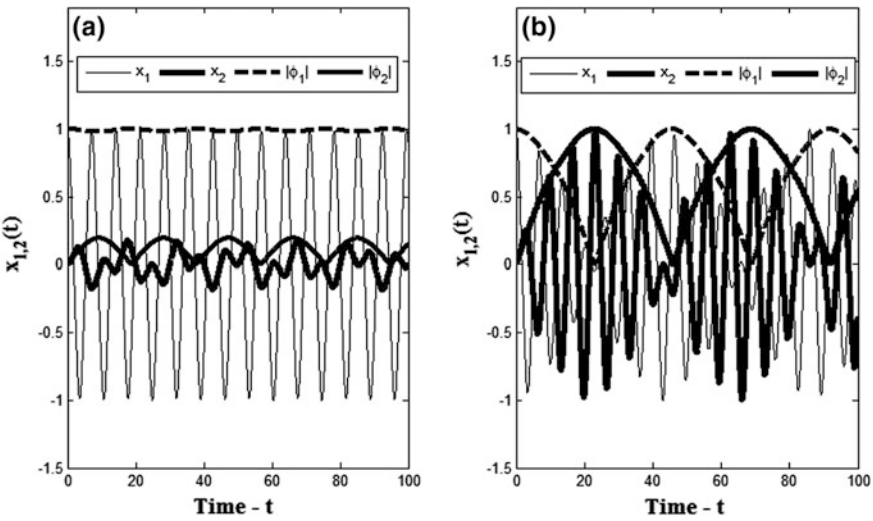

Fig. 2.6 Superposition of the slow envelope (4.4) on the full response (4.1) for $n = 3$ and different coupling strength: **a** $\chi = 0.08 < \chi_{cr}^{(2)}$; **b** $\chi = 0.19 > \chi_{cr}^{(2)}$. Initial conditions: $x_1(0) = 1$, $x_2(0) = 0$; $v_1(0) = v_2(0) = 0$ for the full system; $\varphi_1(0) = i$, $\varphi_2(0) = 0$ for the envelope

To better illustrate the effect of the transition from localization to a complete transport of energy, we construct the Poincaré maps corresponding to system chapter (4.1). To this end, we first restrict the system dynamics to an isoenergetic manifold. It is easy to show that, due to homogeneity of chapter (4.1), the total system energy can be normalized to unity ($E = 1$). Thus, fixing the total energy to a constant level, we restrict the dynamical flow of chapter (5.1) to the three-dimensional isoenergetic manifold $E(x_1, \dot{x}_1, x_2, \dot{x}_2) = 1$. By transversely intersecting the three-dimensional isoenergetic manifold by the two-dimensional cut plane $T : \{x_1 = 0\}$, one obtains the Poincaré map $P : Z \to Z$, where the Poincaré section is defined as.

Fundamental time-periodic solutions of a basic period T correspond to the period 1 equilibrium points in the Poincaré map. Additional subharmonic solutions of periods nT correspond to the period n equilibrium points of the Poincaré map, i.e., to the orbits that pierce the cut section n times before repeating themselves. Clearly, the construction of the Poincaré map $(P : Z \to Z)$ effectively reduces the global system dynamics to the plane (x, v). The Poincaré section in Fig. 2.6a corresponds to the case of $\chi < \chi_{cr}^{(2)}$ (energy localization), while Fig. 2.6b corresponds to the case of $\chi > \chi_{cr}^{(2)}$ (strong beating response).

From the close observation of the results in Fig. 2.7, one can identify the formation of special orbits (marked with bold dots) passing through the origin. It is clear that this invariant set emanating from the origin constitutes a special orbit leading to a complete energy exchange between the oscillators (strong beating response). However, the results in Fig. 2.7a suggest that a similar orbit emanating from the origin do not lead to

complete energy exchange. These special orbits of the Poincaré sections can be directly correlated to the LPT of the reduced model. This special orbit illustrated in Fig. 2.7a corresponds to energy localization (LPT of the first kind) while that one in Fig. 2.7b corresponds to complete energy exchange (LPT of the second kind).

Figures 2.8 and 2.9 present computational results for $n = 7$. Figure 2.8 depicts the time response for $n = 7$. Note that the response of the reduced-order model (2.4) agrees fairly well with the response of the full model (2.1) despite the relatively high power of nonlinearity. The theoretical prediction of the threshold value $\chi_{cr}^{(2)} = 0.0625$ is confirmed in Fig. 2.7.

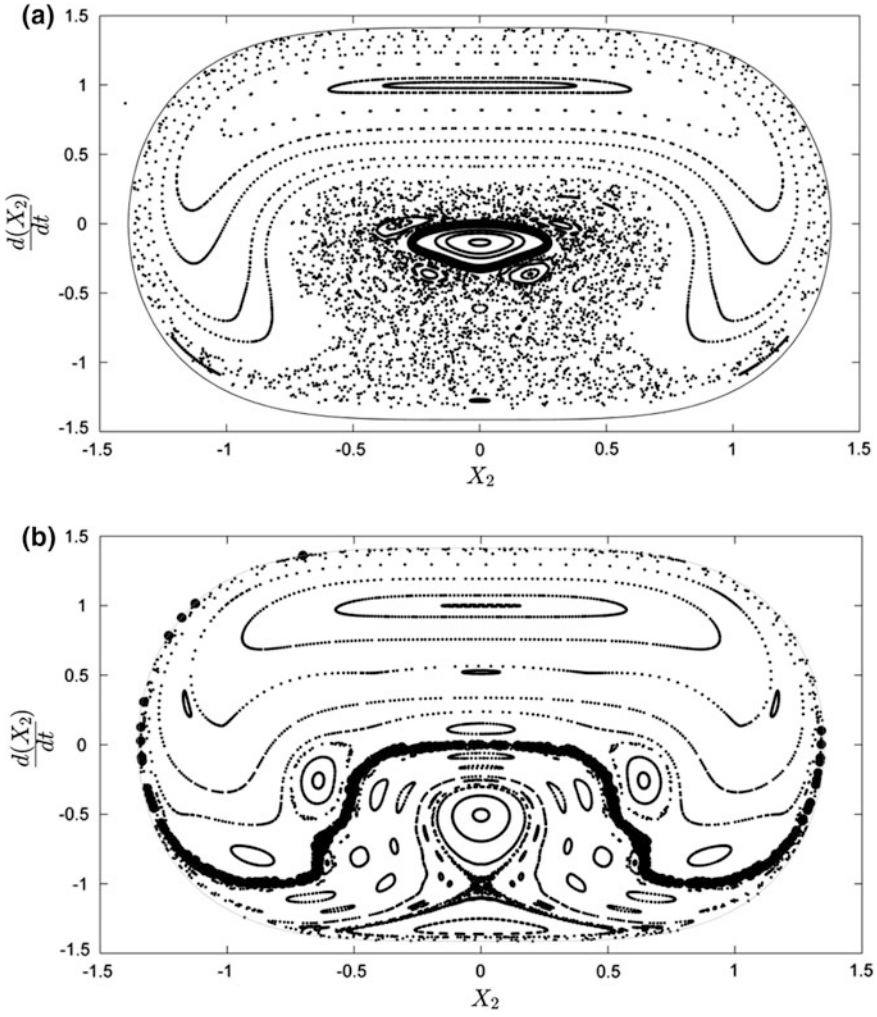

Fig. 2.7 Poincaré map for $n = 3$; $\chi = 0.08 < \chi_{cr}^{(2)}$ (**a**); $\chi = 0.2 > \chi_{cr}^{(2)}$ (**b**). LPT is marked with *bold dots*

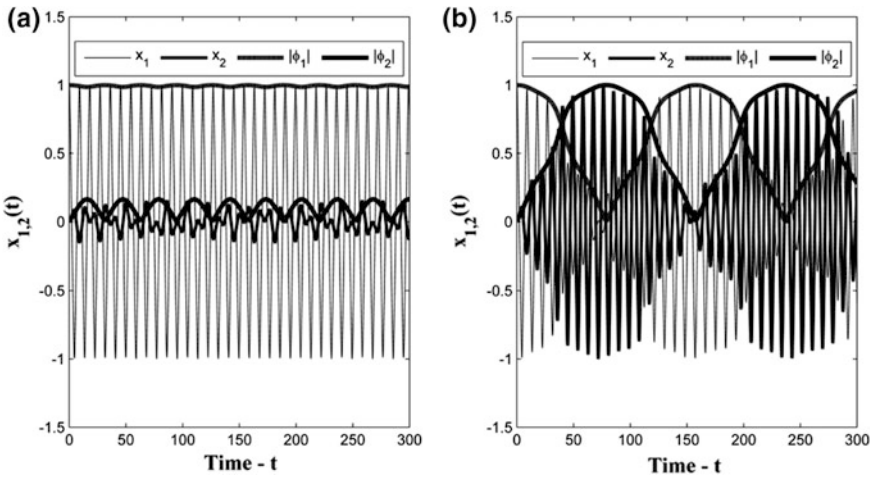

Fig. 2.8 Superposition of the slow envelope (2.4) on the full response (2.1) for $n = 7$ and different coupling strength: **a** $\chi = 0.05 < \chi_{cr}^{(2)}$; **b** $\chi = 0.05 < \chi_{cr}^{(2)}$. Initial conditions are indicated in Fig. 2.6

Figure 2.9 demonstrates that, despite the prevalence of the "chaotic sea" region, which covers almost the entire map, one can still observe the preservation of the special orbits corresponding to the LPTs of the first and the second types.

Numerical simulations show that, with an increase in the coupling parameter χ, the occurrence of the beating response is usually preceded by the regimes of a "mixed" type exhibiting a temporal energy localization followed by distinct irregular transitions into a beating-like response (Fig. 2.10) alternating with subsequent localizations.

In Tables 2.2 and 2.3, we compare the numerically obtained critical values of coupling χ with the theoretically derived values $\chi_{cr}^{(2)}$, $\chi_{cr}^{(3)}$ for different values of n. In numerical simulations, the total system energy is normalized to unity $E = 1$.

Tables 2.2 and 2.3 are constructed for two different initial excitations, namely $x_1(0) = 0$, $v_1(0) = \sqrt{2}$ (Table 2.2) and $x_1(0) = [(n + 1)(1 + \chi)^{-1}]^{1/(n+1)}$, $v_1(0) = 0$ (Table 2.3). We consider the following numerically found critical values of χ: χ_b, corresponding to the breakdown of localization followed by the occurrence of the response of a "mixed" type, and χ_{SB}, related to pure beatings (Fig. 2.11). This "mixed" type of response has been observed in the interval $\chi_b < \chi < \chi_{SB}$, or, in other words, in the interval between energy localization ($\chi < \chi_b$) and beating, associated with complete energy exchange ($\chi > \chi_{SB}$).

An insignificant difference in the critical values χ_b and χ_{SB} in Tables 2.2 and 2.3 can be explained by high sensitivity of system (2.1) to the change of the initial conditions. However, despite these deviations, one can note a good agreement between the numerical and analytical critical values in Tables 2.2 and 2.3.

It is important to note that the formation of regular beatings for $n \geq 9$ is problematic. However, even in the absence of a regular response, one can observe a transition from localization to complete energy exchanges at $\chi = \chi_{cr}^{(2)}$ provided the latter

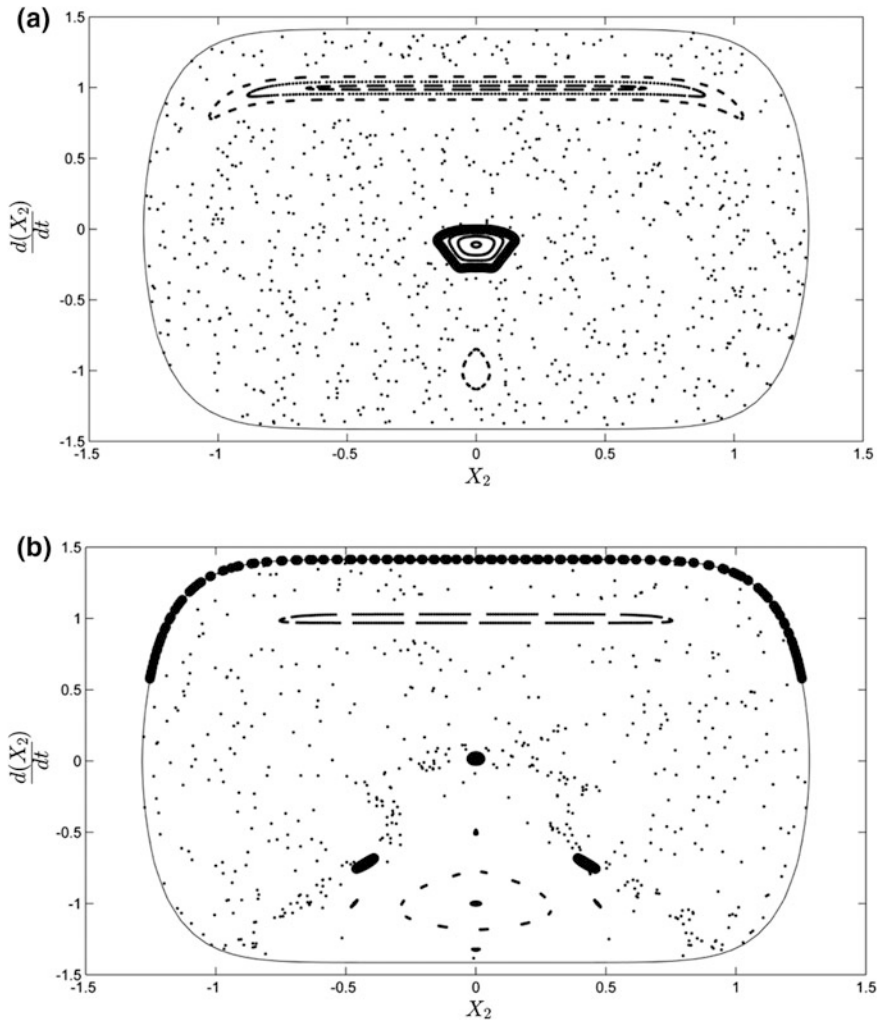

Fig. 2.9 Poincaré map for $n = 7$; $\chi = 0.05 < \chi_{cr}^{(2}$(**a**); $\chi = 0.07 > \chi_{cr}^{(2)}$ (**b**). LPT is marked with *bold dots*

exhibits highly irregular motion, i.e., the chaotic-like behavior. It follows from the results in Tables 2.2 amd 2.3 that, despite the absence of a regular beating response for $n \geq 9$, the analytical model predicts fairly well a critical value χ_b corresponding to the breakdown of localization followed by irregular energy transfer between the oscillators.

If the motion of the particles is transversal to the weightless string itself, the coupling between the particles is realized by the local strongly nonlinear interactions. If the preliminary stretching of the string is absent, they are cubic functions in the main approximation. However, we consider even more general case when the power may be not only three but an arbitrary odd integer.

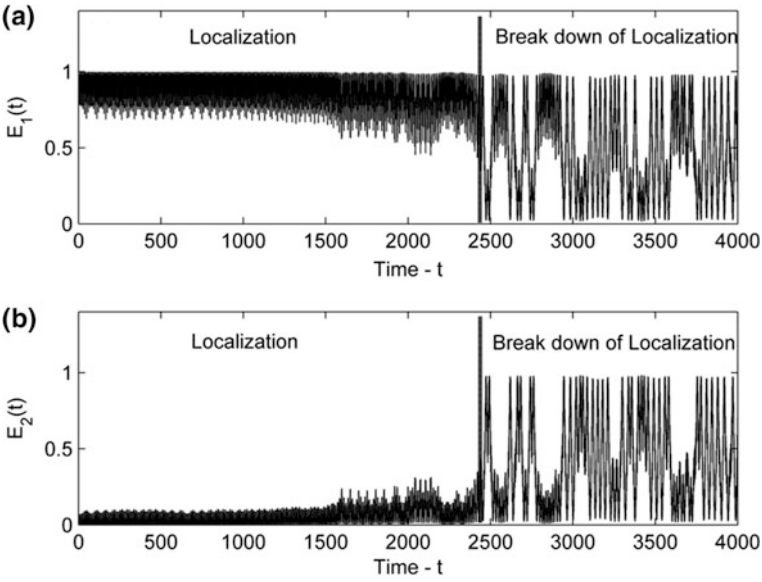

Fig. 2.10 Instantaneous energy corresponding to the mixed type of responses exhibiting temporal localization and sudden bursts of the beating-like behavior ($\chi_b = 0.09$, $n = 3$): **a** energy of the first oscillator; **b** energy of the second oscillator. Initial conditions: $x_1(0) = x_2(0) = 0$; $v_1(0) = \sqrt{2}$, $v_2(0) = 0$

Table 2.2 Comparison of the threshold values $\chi_{cr}^{(2)}$, $\chi_{cr}^{(3)}$ obtained from the theoretical analysis with the critical parameters χ_b, χ_{SB} obtained by numerical calculation of the response of system (2.1) subject to impulse excitation $x_1(0) = x_2(0) = 0$; $v_1(0) = \sqrt{2}$, $v_2(0) = 0$

	$n = 3$	$n = 5$	$n = 7$	$n = 9$	$n = 11$	$n = 13$
$\chi_{cr}^{(2)}$ $(n \leq 5)$ $\chi_{cr}^{(3)}$ $(n \leq 7)$	0.1667	0.1071	0.0625	0.0445	0.0347	0.0285
χ_{SB}	0.17	0.112	0.069	–	–	–
χ_b	0.09	0.0875	0.054	0.038	0.03	0.027

Table 2.3 Comparison of the threshold values $\chi_{cr}^{(2)}$, $\chi_{cr}^{(3)}$ obtained from the theoretical analysis with the critical parameters χ_b, χ_{SB} obtained by numerical calculation of the response of system (2.1) subject to initial displacement $x_1(0) = [(n+1)(1+\chi)^{-1}]^{1/(n+1)}$, $x_2(0) = 0$; $v_1(0) = v_2(0) = 0$

	$n = 3$	$n = 5$	$n = 7$	$n = 9$	$n = 11$	$n = 13$
$\chi_{cr}^{(2)}$	0.1667	0.1071	0.0625	0.0445	0.0347	0.0285
χ_{SB}	0.173	0.11	0.0637	–	–	–
χ_b	0.165	0.108	0.0635	0.044	0.035	0.029

2.2 Non-local Sonic Vacuum

In this section, we remove the restrictions providing purely transversal motion of the particles accepted in the previous section. We formulate the problem for general multiparticle system assuming the presence of lateral springs without a preliminary stretching. However, we discuss here only the result obtained for two-particle model (Kikot et al. 2015), to compare them directly with those for the case of sonic vacuum.

2.2.1 The Model

Considered system is depicted in Fig. 2.11. It consists of n particles of identical mass m connected by linear inter-chain springs of elastic constant k_1; moreover, each particle is connected to the ground by two linear lateral springs of elastic constant k_2. It is assumed that all particles perform in-plane oscillations on the vertical plane (Oxy), and that all springs are unstretched at the equilibrium of the system corresponding to the line $y = z = 0$ (see Fig. 2.11). In addition, fixed-fixed boundary conditions are assumed for the particle chain, the unstretched length of the i-th inter-chain spring connecting particles $i-1$ and i is being taken equal to l_i, for $i = 1, 2, \ldots, n$, and the unstretched lengths of the lateral springs are assumed to be equal to d. Considering the free in-plane oscillations of this system, the transverse and axial deformations of particle i are denoted by v_i and u_i, respectively, and the deformed length of the i-th inter-chain spring by l_i' and of the i-th lateral springs by d_i' (both lateral springs have equal stretched lengths due to symmetry). Without loss of generality gravity forces are disregarded, and it is assumed that no dissipation forces exist. Finally, without loss of generality, the normalization $\sum_{i=1}^{n+1} l_i = 1$ is imposed for the inter-chain springs. Then, the analysis follows the approach developed in (Manevitch and Vakakis 2014) for the corresponding system with no lateral grounding supports.

Applying Newton's law in the vertical and transverse directions, the equations of motion of i-th particle are expressed as,

$$\begin{aligned} m\ddot{u}_i + T_i \cos\phi_i - T_{i+1}\cos\phi_{i+1} + S_i \sin\theta_i \sin\psi_i = 0 \\ m\ddot{v}_i + T_i \sin\phi_i - T_{i+1}\sin\phi_{i+1} + S_i \sin\theta_i \cos\psi_i = 0 \end{aligned} \tag{2.20}$$

where $T_i = k_1\left(l_i' - l_i\right)$ and $S_i = k_2\left(d_i' - d\right)$ are the stretching forces (tensions) in the i-th inter-chain and lateral springs, respectively, ϕ_i is the angle between the i-th spring and the horizontal direction, θ_i is the angle between the deformed and undeformed positions of the i-th lateral springs, $\psi_i = \tan^{-1}(u_i/v_i)$, overdots denote differentiation with respect to the temporal variable t, and $i = 1, 2, \ldots, n$. At this

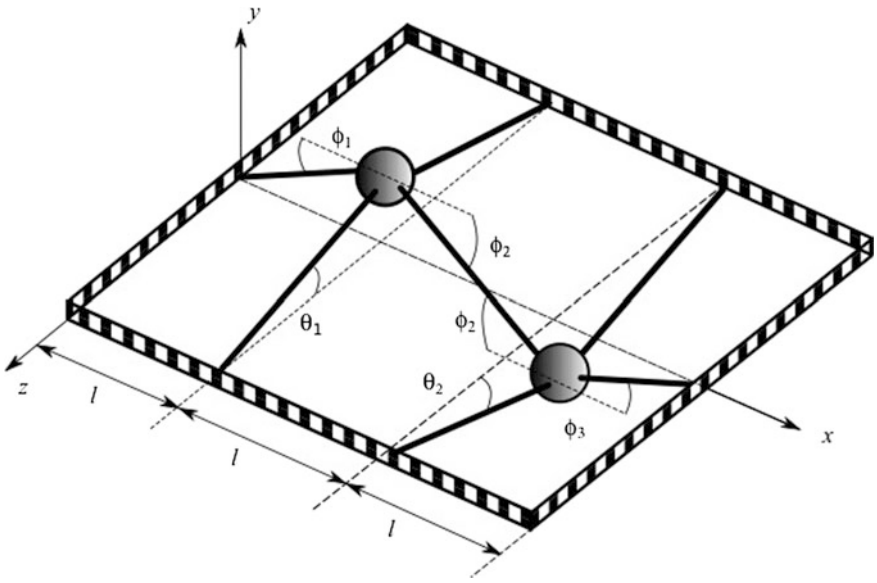

Fig. 2.11 Model of grounded nonlinear sonic vacuum consisting of 2 particles performing in-plane oscillations on the (*Oxy*) plane; the unstretched spring are depicted by *solid lines* and their undeformed states are shown by the *dashed lines*; l is the length of the springs; other notation—see text below

point, the elongation of the i-th inter-chain spring, $\varepsilon_{1i} = \left(l_i' - l_i\right)/l_i$, and the elongation $\varepsilon_{2i} = \left(d_i' - d\right)/d$ of the i-th lateral springs are introduced, and *the limiting case corresponding to predominantly low-energy transversal oscillations is considered*, taking into account only the corresponding leading-order geometrically nonlinear effects in the oscillating chain.

Accordingly, the trigonometric expressions in (2.20) are expressed in terms of the particle displacements v_i and u_i through the following geometric relations,

$$\begin{aligned} \cos\phi_i &= \frac{l_i + u_i - u_{i-1}}{\left[\left(v_i - v_{i-1}\right)^2 + \left(l_i + u_i - u_{i-1}\right)^2\right]^{\frac{1}{2}}} \\ \sin\phi_i &= \frac{v_i - v_{i-1}}{\left[\left(v_i - v_{i-1}\right)^2 + \left(l_{i-1} + u_i - u_{i-1}\right)^2\right]^{\frac{1}{2}}} \end{aligned} \tag{2.21a}$$

$$\sin\theta_i = \frac{\left(u_i^2 + v_i^2\right)^{\frac{1}{2}}}{\left[u_i^2 + v_i^2 + d^2\right]^{\frac{1}{2}}} \tag{2.21b}$$

$$\begin{aligned}\cos\psi_i &= \frac{v_i}{\left[u_i^2+v_i^2\right]^{\frac{1}{2}}}\\ \sin\psi_i &= \frac{u_i}{\left[u_i^2+v_i^2\right]^{\frac{1}{2}}}\end{aligned} \tag{2.21c}$$

and the spring deformations by,

$$l_i'-l_i=\left[(v_i-v_{i-1})^2+(l_i+u_i-u_{i-1})^2\right]^{1/2}-l_i \tag{2.22a}$$

$$d_i'-d=\left[u_i^2+v_i^2+d^2\right]^{1/2}-d \tag{2.22b}$$

We will be interested in the limit of low-energy oscillations and sufficiently small angles ϕ_i, θ_i and ψ_i. Specifically, we will assume that the amplitudes of the transverse oscillations of the particles are much smaller than the axial distances (on the x-axis) between them; accordingly, we introduce the normalized displacements $\bar{u}_i = u_i/l$ and $\bar{v}_i = v_i/l$, and rescale the normalized displacements according to $\bar{u}_i \to \varepsilon^2\bar{u}_i$ and $\bar{v}_i \to \varepsilon\bar{v}_i$. The small parameter $\varepsilon \ll 1$ is introduced to indicate the smallness of the transverse and axial normalized deformations and will be regarded as the small parameter in the perturbation analysis that follows. Moreover, we introduce the *slow timescale* $\tilde{t} = \varepsilon(k_1/m)^{1/2}t$ and assume for simplicity that $l_i = l = 1/(n+1),\ \ i = 0, 1, \ldots, n+1$. Note that by the above rescalings, the axial displacements are assumed to be an order of magnitude smaller compared to the transverse ones.

Substituting these normalizations and rescalings into expressions (2.21a)–(2.21c) and (2.22a), (2.22b), omitting the overbars from the normalized displacements, and expanding in Taylor series with respect to the small parameter, we derive the following leading-order approximations that are valid in the low-energy limit:

$$\begin{aligned}\varepsilon_{1i} &= \varepsilon^2\left[(u_i-u_{i-1})+\frac{1}{2}(v_i-v_{i-1})^2\right]+\cdots, \quad T_i = k_1 l\varepsilon_{1i}\\ \varepsilon_{2i} &= \left(\frac{\varepsilon^2 l^2}{2d^2}\right)v_i^2+\cdots, \quad S_i = k_2 d\varepsilon_{2i}\\ \cos\phi_i &= 1+\cdots, \quad \sin\phi_i = \varepsilon(v_i-v_{i-1})+\cdots\\ \sin\theta_i &= \left(\frac{\varepsilon l}{d}\right)v_i+\cdots\\ \cos\psi_i &= 1+\cdots, \quad \sin\psi_i = \frac{\varepsilon u_i}{v_i}+\cdots\end{aligned} \tag{2.23}$$

In turn, substituting (2.23) into the equations of motion (2.20) governing the axial and transverse oscillations of the particles, we derive the following leading-order approximate equations valid in the low-energy limit:

$$\varepsilon^2 u_i'' + (2u_i - u_{i+1} - u_{i-1}) - \frac{1}{2}(v_{i+1} - v_i)^2 + \frac{1}{2}(v_i - v_{i-1})^2 + \mathcal{O}(\varepsilon^2) = 0 \tag{2.24a}$$

$$\begin{aligned} & v_i'' - (u_{i+1} - u_i)(v_{i+1} - v_i) \\ & \quad - \frac{1}{2}(v_{i+1} - v_i)^3 + (u_i - u_{i-1})(v_i - v_{i-1}) + \frac{1}{2}(v_i - v_{i-1})^3 + Cv_i^3 + \mathcal{O}(\varepsilon^2) \\ & \quad = 0 \end{aligned} \tag{2.24b}$$

with $i = 1, \ldots, n$, $C = \left(\frac{k_2 l^2}{2k_1 d^2}\right)$, and prime denoting differentiation with respect to the slow timescale $\tilde{t}$.

We now express the Eqs. (2.24a) governing the $\mathcal{O}(\varepsilon^2)$ axial oscillations in terms of the axial tension developing in the chain,

$$\varepsilon^2 u_i'' + \bar{T}_i - \bar{T}_{i+1} + \cdots = 0 \tag{2.25}$$

where $\bar{T}_i$ denotes the rescaled tension in the i-th spring (after the previous normalizations and rescalings are imposed on the unscaled variable T_i), and with the understanding that $u_0 = u_{n+1} \equiv 0$ and $v_0 = v_{n+1} \equiv 0$ due to the fixed-fixed boundary conditions. Both (2.24a) and (2.25) are in singular form since in the limit $\varepsilon \to 0$ the derivative term vanishes, which enables the partition of the axial dynamics in terms of slow and fast components and the asymptotic treatment of the dynamics. Indeed, in the leading-order "slow" approximation with $\varepsilon = 0$, we may neglect the axial inertial effects in the dynamics to obtain $\bar{T}_1 = \bar{T}_2 = \cdots = \bar{T}_{n+1} \equiv \bar{T}$, which indicates that to leading-order, the rescaled tension in the springs is spatially uniform. In physical terms, this means that in slow timescale τ_1, the axial oscillations are relatively fast, so that an axial disturbance generated at a point of the chain propagates quickly to the remainder of the system. As a result, we can derive the following *non-local* representation of the average axial force in the low-energy limit:

$$\begin{aligned} \bar{T} &= \frac{1}{n+1}\sum_{p=1}^{n+1} \bar{T}_p = \frac{1}{n+1}\sum_{q=0}^{n}\left[(u_{q+1} - u_q) + \frac{1}{2}(v_{q+1} - v_q)^2\right] \\ &= \frac{1}{2(n+1)}\sum_{q=0}^{n}(v_{q+1} - v_q)^2 \end{aligned} \tag{2.26}$$

since $u_0 = u_{n+1} \equiv 0$. Note that the tension is uniform in the slow timescale, but when higher-order terms are taken into account, it becomes slowly varying (and not uniform) in space. This is equivalent to considering only the outer solutions in the axial equations of motion (2.24a) by neglecting the derivative term (or, setting $\varepsilon^2 = 0$) and deriving the following approximate (slow) expression,

$(2u_i - u_{i+1} - u_{i-1}) \approx \frac{1}{2}(v_{i+1} - v_i)^2 - \frac{1}{2}(v_i - v_{i-1})^2$, which combined with (2.26) brings the equations governing the transverse oscillations (2.24b) in the form:

$$\begin{aligned} &\mu v_i''(\tilde{t}) + \mu \bar{T}[\underline{v}(\tilde{t})][2v_i(\tilde{t}) - v_{i+1}(\tilde{t}) - v_{i-1}(\tilde{t})] + v_i^3(\tilde{t}) + \cdots = 0, \quad i = 1, \ldots, n \\ &v_0 = v_{n+1} \equiv 0 \end{aligned} \tag{2.27}$$

where $\bar{T}[\underline{v}(\tilde{t})] \equiv \frac{1}{2(n+1)}\left[\sum_{q=0}^{n}(v_{q+1}(\tilde{t}) - v_q(\tilde{t}))^2\right]$ is a quadratic term depending on the transverse displacement vector $\underline{v}(\tau) = [\, v_1 \quad \ldots \quad v_N \,]^T$, and $\mu \equiv C^{-1} = \left(\frac{2k_1 d^2}{k_2 l^2}\right)$. The average longitudinal force may be regarded as a non-local force that is generated through the elastic extension of the chain by Hooke's law. The dynamical system (2.27) governs the leading-order slow transverse oscillations of the particles and is studied in detail in Sect. 2.3.

Considering the structure of the coupled oscillators (2.27), we note that there is complete absence of any linear stiffness component since all terms (except the inertia term) are of the third order. Accordingly, this system represents a nonlinear sonic vacuum since the linearized speed of sound in this medium is zero. Furthermore, similar to the nonlinear sonic vacuum derived in (Manevitch and Vakakis 2014), the system (2.27) governing the transverse oscillations of the particles contains strongly non-local terms even though starting system of Eqs. 2.20 involves only next-neighbor physical coupling between particles.

In the following analysis, we will consider system Eq. (2.27) in its simplest form corresponding to $n = 2$ in an attempt to highlight the highly complex dynamics that this system possesses. Following to the asymptotic treatment of the slow transverse oscillations of the chain, we will reconsider the axial oscillations governed by Eq. (2.24a) or Eq. (2.25) which will be shown to possess both slow and fast components.

2.2.2 *Two-Particle System (n = 2): Slow Transverse Oscillations*

For $n = 2$ system (2.27) reads,

$$\begin{aligned} \mu v_1'' + \tfrac{\mu}{6}\left[v_1^2 + (v_2 - v_1)^2 + v_2^2\right](2v_1 - v_2) + v_1^3 + \cdots = 0 \\ \mu v_2'' + \tfrac{\mu}{6}\left[v_1^2 + (v_2 - v_1)^2 + v_2^2\right](2v_2 - v_1) + v_2^3 + \cdots = 0 \end{aligned} \tag{2.28}$$

and is in the form of two strongly nonlinear coupled oscillators. It can be also obtained directly from the variation of the following Lagrange function:

$$L = \frac{\dot{v}_1^2 + \dot{v}_2^2}{2} - \left[\frac{1}{4\mu}\left(v_1^4 + v_2^4\right) - \frac{1}{6}\left(v_1^4 + v_2^4 - 2v_2^3 v_1 - 2v_1^3 v_2 + 3v_1^2 v_2^2\right)\right]$$

Given that this system is homogeneous in its nonlinear terms, it admits similar nonlinear normal modes, i.e., time periodic oscillations corresponding to straight lines in the configuration plane (v_1, v_2). To compute them, we impose the linear relationship between the two coordinates, $v_2 = kv_1$, and substitute into (2.28) to find the modal constant k by the algebraic relation:

$$k\left\{1 + \frac{\mu}{6}\left[1 + (k-1)^2 + k^2\right](2-k)\right\} = k^3 + \frac{\mu}{6}\left[1 + (k-1)^2 + k^2\right](2k-1) \tag{2.29a}$$

There are always the solutions $k_{1,2} = \pm 1$ which correspond to in-phase and out-of-phase NNMs resulting due to the symmetry of the system. Two additional solutions are given by,

$$k_{3,4} = \frac{\mu - 3 \pm \sqrt{(\mu-3)^2 - 4\mu^2}}{2\mu} < 0$$

provided that $0 < \varepsilon < \mu < 1$ (note that if $\mu < \varepsilon$, we cannot separate transversal from longitudinal motions through the previous rescalings). This indicates that at $\mu = 1$, a bifurcation of the out-of-phase similar NNM takes place, generating two additional out-of-phase NNMs; this pitchfork bifurcation, together with other strongly nonlinear and non-stationary dynamical phenomena that can occur in system (2.28), will be studied in more detail in the following asymptotic analysis.

For each NNM, the leading-order approximations to the transverse displacements are computed by solving by quadratures the nonlinear equations for modal oscillators,

$$\begin{aligned} &v_1'' + \left\{\frac{1}{6}\left[1 + (k-1)^2 + k^2\right](2-k) + (1/\mu)\right\} v_1^3 + \cdots = 0, \\ &v_2 = kv_1 \end{aligned} \tag{2.29b}$$

under the specified initial conditions of the problem.

2.2.3 Slow Flow Reduction of the Dynamics

We resort to a complexification/averaging methodology to analytically study its stationary and non-stationary resonance dynamics. To this end, we rewrite this system as,

$$\begin{aligned}\mu\left(v_1''+\omega^2 v_1\right)+\varepsilon_1\gamma\left\{v_1^3-\mu\omega^2 v_1+\tfrac{\mu}{6}\left[v_1^2+(v_2-v_1)^2+v_2^2\right](2v_1-v_2)\right\}+\cdots=0\\ \mu\left(v_2''+\omega^2 v_2\right)+\varepsilon_1\gamma\left\{v_2^3-\mu\omega^2 v_2+\tfrac{\mu}{6}\left[v_1^2+(v_2-v_1)^2+v_2^2\right](2v_2-v_1)\right\}+\cdots=0\end{aligned} \tag{2.30}$$

where $\gamma = 1/\varepsilon_1$ and ε_1 are bookkeeping parameters used in the following asymptotic analysis, $\omega = (k_1/m)^{1/2}$, and identical terms were added and subtracted in the two equations. Then, we complexify the analysis by introducing the new complex variables,

$$\psi_1 = v_1' + j\omega v_1, \psi_2 = v_2' + j\omega v_2, j = (-1)^{1/2}$$

and the difference $\Phi = \psi_1 - \psi_2$. Expressing (2.11) in terms of the new complex variables, we obtain,

$$\begin{aligned}\mu\left(\psi_1' - j\omega\psi_1\right) = -\varepsilon_1\gamma\Bigg\{&\left(\frac{\psi_1-\psi_1^*}{2j\omega}\right)^3+\frac{\mu}{6}\left[\left(\frac{\psi_1-\psi_1^*}{2j\omega}\right)^2+\left(\frac{\phi-\phi^*}{2j\omega}\right)^2+\left(\frac{\psi_2-\psi_2^*}{2j\omega}\right)^2\right]\\ &\times\left(2\frac{\psi_1-\psi_1^*}{2j\omega}-\frac{\psi_2-\psi_2^*}{2j\omega}\right)+\frac{j\mu\omega}{2}\left(\psi_1-\psi_1^*\right)\Bigg\}\\ \mu\left(\psi_2' - j\omega\psi_2\right) = -\varepsilon_1\gamma\Bigg\{&\left(\frac{\psi_2-\psi_2^*}{2j\omega}\right)^3+\frac{\mu}{6}\left[\left(\frac{\psi_1-\psi_1^*}{2j\omega}\right)^2+\left(\frac{\phi-\phi^*}{2j\omega}\right)^2+\left(\frac{\psi_2-\psi_2^*}{2j\omega}\right)^2\right]\\ &\times\left(2\frac{\psi_2-\psi_2^*}{2j\omega}-\frac{\psi_1-\psi_1^*}{2j\omega}\right)+\frac{j\mu\omega}{2}\left(\psi_2-\psi_2^*\right)\Bigg\}\end{aligned} \tag{2.31}$$

where $(\cdot)^*$ denotes complex conjugate. System (2.31) is now analyzed by applying the method of multiple scales by introducing the new timescales $\tilde{t}_0 = \tilde{t}, \tilde{t}_1 = \varepsilon_1\tilde{t}$, $\tilde{t}_2 = \varepsilon_1^2\tilde{t}, \ldots$ and considering the asymptotic expansions $\psi_i(\tilde{t}) = \psi_{i0}(\tilde{t}_0, \tilde{t}_1, \tilde{t}_2, \ldots)$ $+ \varepsilon_1\psi_{i1}(\tilde{t}_0, \tilde{t}_1, \tilde{t}_2, \ldots) + \varepsilon_1^2\psi_{i2}(\tilde{t}_0, \tilde{t}_1, \tilde{t}_2, \ldots) + \cdots, i = 1, 2$. Substituting in (2.31), expressing the time derivatives in terms of the new timescales and matching coefficients at different orders of ε_1, we obtain an hierarchy of subproblems governing the solutions of (2.31) at progressively higher of approximation. Since the following analysis will be restricted only up to terms of $\mathcal{O}(\varepsilon_1)$, only the two leading timescales will be considered.

The zeroth order approximation is obtained by matching coefficients of $\mathcal{O}(\varepsilon_1^0)$ and solving the following subproblem:

$$\frac{\partial\psi_{i0}(\tilde{t}_0,\tilde{t}_1)}{\partial\tilde{t}_0} - j\omega\psi_{i0}(\tilde{t}_0,\tilde{t}_1) = 0 \Rightarrow \psi_{i0}(\tilde{t}_0,\tilde{t}_1) = \varphi_{i0}(\tilde{t}_1)e^{j\omega\tilde{t}_0}, \quad i = 1, 2 \tag{2.32}$$

This provides the leading-order approximation to the solution and indicates that at the basic approximation, both particles perform slowly modulated transverse oscillations with common fast frequency ω. Hence, the following analysis is carried out under the assumption of 1:1 resonance in terms of the transverse oscillations, and all stationary and non-stationary dynamics discussed below satisfy this 1:1 resonance condition. The slowly varying complex amplitudes $\varphi_{i0}(\tilde{t}_1)$ are computed by substituting (2.32) into the problem governing the $\mathcal{O}(\varepsilon_1^1)$ approximation,

$$
\begin{aligned}
\mu\frac{\partial\psi_{11}}{\partial\tilde{t}_0}-j\mu\omega\psi_{11} &= -\mu\frac{\partial\varphi_{10}}{\partial\tilde{t}_1}-\gamma\Bigg\{\left(\frac{\varphi_{10}\mathrm{e}^{j\omega\tilde{t}_0}-\varphi_{10}^{*}\mathrm{e}^{-j\omega\tilde{t}_0}}{2j\omega}\right)^3\\
&\quad+\frac{\mu}{6}\Bigg[\left(\frac{\varphi_{10}\mathrm{e}^{j\omega\tilde{t}_0}-\varphi_{10}^{*}\mathrm{e}^{-j\omega\tilde{t}_0}}{2j\omega}\right)^2+\left(\frac{\Phi_0-\Phi_0^{*}}{2j\omega}\right)^2\\
&\quad+\left(\frac{\varphi_{20}\mathrm{e}^{j\omega\tilde{t}_0}-\varphi_{20}^{*}\mathrm{e}^{-j\omega\tilde{t}_0}}{2j\omega}\right)^2\Bigg]\\
&\quad\times\left(\frac{\varphi_{10}\mathrm{e}^{j\omega\tilde{t}_0}-\varphi_{10}^{*}\mathrm{e}^{-j\omega\tilde{t}_0}}{j\omega}-\frac{\varphi_{20}\mathrm{e}^{j\omega\tilde{t}_0}-\varphi_{20}^{*}\mathrm{e}^{-j\omega\tilde{t}_0}}{2j\omega}\right)\\
&\quad+\frac{j\mu\omega\left(\varphi_{10}\mathrm{e}^{j\omega\tilde{t}_0}-\varphi_{10}^{*}\mathrm{e}^{-j\omega\tilde{t}_0}\right)}{2}\Bigg\}\\
\mu\frac{\partial\psi_{21}}{\partial\tilde{t}_0}-j\mu\omega\psi_{21} &= -\mu\frac{\partial\varphi_{20}}{\partial\tilde{t}_1}-\gamma\Bigg\{\left(\frac{\varphi_{20}\mathrm{e}^{j\omega\tilde{t}_0}-\varphi_{20}^{*}\mathrm{e}^{-j\omega\tilde{t}_0}}{2j\omega}\right)^3\\
&\quad+\frac{\mu}{6}\Bigg[\left(\frac{\varphi_{10}\mathrm{e}^{j\omega\tilde{t}_0}-\varphi_{10}^{*}\mathrm{e}^{-j\omega\tilde{t}_0}}{2j\omega}\right)^2+\left(\frac{\Phi_0-\Phi_0^{*}}{2j\omega}\right)^2\\
&\quad+\left(\frac{\varphi_{20}\mathrm{e}^{j\omega\tilde{t}_0}-\varphi_{20}^{*}\mathrm{e}^{-j\omega\tilde{t}_0}}{2j\omega}\right)^2\Bigg]\\
&\quad\times\left(\frac{\varphi_{20}\mathrm{e}^{j\omega\tilde{t}_0}-\varphi_{20}^{*}\mathrm{e}^{-j\omega\tilde{t}_0}}{j\omega}-\frac{\varphi_{10}\mathrm{e}^{j\omega\tilde{t}_0}-\varphi_{10}^{*}\mathrm{e}^{-j\omega\tilde{t}_0}}{2j\omega}\right)\\
&\quad+\frac{j\mu\omega\left(\varphi_{20}\mathrm{e}^{j\omega\tilde{t}_0}-\varphi_{20}^{*}\mathrm{e}^{-j(2.2.13)\omega\tilde{t}_0}\right)}{2}\Bigg\}
\end{aligned}
\tag{2.33}
$$

and eliminating secular terms proportional to $\mathrm{e}^{j\omega\tilde{t}_0}$ from the right-hand sides which render the $\mathcal{O}(\varepsilon_1^1)$ approximations non-uniformly valid in the timescale $\tilde{t}_0$. This results in the following set of slowly modulated complex equations in the timescale $\tilde{t}_1$:

$$\mu\frac{\partial\varphi_{10}}{\partial\tilde{t}_1}=\gamma\Bigg\{\frac{3j\varphi_{10}|\varphi_{10}|^2}{8\omega^3}-\frac{j\mu\omega\varphi_{10}}{2}+\frac{j\mu\Big[\varphi_{10}^2+(\varphi_{10}-\varphi_{20})^2+\varphi_{20}^2\Big](2\varphi_{10}^*-\varphi_{20}^*)}{48\omega^3}$$
$$+\frac{j\mu\Big[|\varphi_{10}|^2+|\varphi_{10}-\varphi_{20}|^2+|\varphi_{20}|^2\Big](2\varphi_{10}-\varphi_{20})}{24\omega^3}\Bigg\}$$
$$\mu\frac{\partial\varphi_{20}}{\partial\tilde{t}_1}=\gamma\Bigg\{\frac{3j\varphi_{20}|\varphi_{20}|^2}{8\omega^3}-\frac{j\mu\omega\varphi_{20}}{2}+\frac{j\mu\Big[\varphi_{10}^2+(\varphi_{10}-\varphi_{20})^2+\varphi_{20}^2\Big](2\varphi_{20}^*-\varphi_{10}^*)}{48\omega^3}$$
$$+\frac{j\mu\Big[|\varphi_{10}|^2+|\varphi_{10}-\varphi_{20}|^2+|\varphi_{20}|^2\Big](2\varphi_{20}-\varphi_{10})}{24\omega^3}\Bigg\} \tag{2.34}$$

This represents the *complex slow flow* of the dynamics of system (2.28). As shown below, it is fully integrable and, hence, analytically solvable since it possesses two first integrals of motion. This indicates that the slow dynamics at the timescale $\tilde{t}_1$ can be exactly determined.

A first integral of the slow flow (2.34) is reflecting energy conservation and is given by

$$|\varphi_{10}(\tilde{t}_1)|^2+|\varphi_{20}(\tilde{t}_1)|^2=N \tag{2.35}$$

To compute a second independent first integral of motion, we express the slow flow (2.34) in terms of real variables by introducing the following polar transformations:

$$\varphi_{10}=\sqrt{N}\,\cos\theta\,\mathrm{e}^{j\delta_1}\quad\text{and}\quad\varphi_{20}=\sqrt{N}\,\sin\theta\,\mathrm{e}^{j\delta_2} \tag{2.36}$$

Substituting (2.36) into (2.34), setting separately the real and imaginary parts equal to zero, and manipulating the resulting equations, we obtain the following equations which represent the slow flow of the dynamics of system (2.28) in real coordinates, on the isoenergetic manifold $N=N_0$:

$$\frac{\mathrm{d}\theta}{\mathrm{d}\tilde{t}_1}=\frac{3\gamma N_0}{48\omega^3}(\sin 2\theta\quad\sin 2\Delta-2\sin\Delta) \tag{2.37a}$$

$$\mu\,\sin\theta\,\cos\theta\,\frac{\mathrm{d}\Delta}{\mathrm{d}\tilde{t}_1}=-\frac{3\gamma N_0}{32\omega^3}\sin 4\theta+\frac{\gamma\mu N_0}{24\omega^3}\left(\frac{3}{4}\,\sin 4\theta\,\cos 2\Delta 3\,\cos 2\theta\,\cos\Delta\right) \tag{2.37b}$$

where $\Delta=\delta_2-\delta_1$. In particular, system (2.37a) and (2.37b) represents a reduction of the dynamics on the *isoenergetic slow flow two-torus* $(\theta,\Delta)\in[0,\pi/2]\times[0,\pi]$.

2.2.4 Stationary and Non-stationary Dynamics

The stationary (time periodic) solutions of system (2.28) correspond to $\frac{d\theta}{d\tilde{t}_1} = \frac{d\Delta}{d\tilde{t}_1} = 0$, since this leads to constant-amplitude fast oscillations of the leading-order approximations (2.32). It can be easily shown that $(\theta_e, \Delta_e) = (\pi/4, 0)$ is an equilibrium point on the torus corresponding to the in-phase similar NNM with modal constant $k_1 = 1$; the resulting solutions of system (2.28) are given by $v_1(\tilde{t}) = v_2(\tilde{t}) = A\ \sin(\omega\tilde{t} + \delta_1) + \mathcal{O}(\varepsilon)$, where the amplitude A and phase δ_1 are determined by the initial conditions. Similarly, the equilibrium point $(\theta_e, \Delta_e) = (\pi/4, \pi)$ corresponds to the out-of-phase similar NNM with $k_2 = -1$ with solutions $v_1(\tilde{t}) = -v_2(\tilde{t}) = A\ \sin(\omega\tilde{t} + \delta_1) + \mathcal{O}(\varepsilon)$. Additional equilibrium solutions (NNMs) correspond to $\sin 2\theta\ \sin 2\Delta - 2\ \sin\Delta = 0$, which leads to two additional equilibrium positions $(\theta_e, \Delta_e) = \left(\theta^*_{e1,2}, \pi\right)$, where $\theta^*_{e1,2}$ are the two real roots of $\sin 2\theta = -2\mu/(\mu - 3)$ for $\mu < 1$; these correspond to the two bifurcating similar NNMs with modal constants $k_3, k_4 < 0$.

To study the non-stationary dynamics of system (2.28) and investigate changes in the global dynamics due to the previous bifurcation of NNMs, we reconsider the reduced slow flow on the isoenergetic two-torus (2.37a), (2.37b), and rescale the slow timescale as $\tilde{t}_1 = \frac{\gamma N_0}{32\omega^3}\tilde{t}_1$ to express it in the following simpler form:

$$\frac{d\theta}{d\tilde{t}_1} = 2(\sin 2\theta\ \sin 2\Delta - 2\ \sin\Delta) \tag{2.38a}$$

$$\frac{d\Delta}{d\tilde{t}_1} = \frac{2}{\mu\ \sin 2\theta}[-3\ \sin 4\theta + \mu\ (\sin 4\theta\ \cos 2\Delta - 4\ \cos 2\theta\ \cos\Delta)] \tag{2.38b}$$

It can be shown that this system has the first integral of motion,

$$\mu\left(\frac{1}{2}\ \sin^2 2\theta\ \cos 2\Delta - 2\ \ \sin 2\theta\ \cos\Delta\right) + \frac{3}{4}\ \cos 4\theta = H \tag{2.39}$$

which enables the exact analytic solution of system (2.38a), (2.38b). This represents a second independent first integral of motion of the slow flow (2.34), in addition to the energy-conservation first integral (2.35). Before proceeding to a more detailed analytical treatment of the dynamics on the two-torus (2.38a) and (2.38b) we discuss the bifurcations that occur in this system as the parameter μ changes.

There are two critical values for the parameter μ corresponding to two bifurcations affecting the stationary and non-stationary dynamics on the two-torus Eqs. (2.38a) and (2.38b). The first critical value, $\mu_{c1} = 1$, is the point of the pitchfork bifurcation of the out-of-phase NNM discussed in the introduction of this section, whereas the second critical value is concerned with a bifurcation of a *limiting phase trajectory* and the occurrence of strong energy exchanges between the coupled oscillators Eq. (2.28). As shown, a unified description of highly

non-stationary resonance dynamics can be performed by introducing the concept of LPT. In fact, the LPT may be regarded as the orbit that is "maximally distant" from the stationary points (NNMs) on the two-torus (2.38a and 2.38b) and passes through the point $(\theta, \Delta) = (0, 0)$. In that context, the second critical value, $\mu = \mu_{c2}$, corresponds to the point where an LPT of the slow flow coincides with a separatrix, after which its topological structure changes drastically and from spatially extended becomes spatially localized. As shown in the numerical results presented below, critical value of orbits of the slow flow (2.38a and 2.38b) passing through the points $(\theta, \Delta) = (0, 0)$ and $(\pi/4, \pi)$ corresponds to the same value of the first integral Eq. (2.39). This estimates the second critical value as $\mu_{c2} = 0.6$.

The aforementioned transitions of the non-stationary dynamics of system Eq. (2.28) are depicted in Fig. 2.11 where the slow flow on the isoenergetic two-torus Eqs. (2.38a) and (2.38b) is depicted for varying values of μ. These results illustrate the transition of the dynamics of system (2.28) from complete energy exchanges between the two oscillators and energy localization in one of these oscillators. For $\mu > \mu_{c1}$, the torus possesses two stable similar NNMs, whereas after the NNM bifurcation at $\mu = \mu_{c1}$, there are four similar NNMs, with the out-of-phase NNM becoming unstable and the other NNMs being stable. The instability of the out-of-phase NNM for $\mu < \mu_{c1}$ affects drastically the global stationary dynamics on the two-torus since it generates two additional NNMs and two homoclinic loops (separatrices) that emanate from the unstable mode. However, the full energy exchange described by LPTs still remains possible. *Key to understanding non-stationary, resonant energy exchanges between the two coupled oscillators (Eq. (9)) is the topological changes of the LPTs* in Fig. 2.12 as μ varies. For $\mu > \mu_{c2}$, there occur strong energy exchanges along an LPT of the system, signified by strongly modulated transverse oscillations of the two particles of the system (or nonlinear beat phenomena). This is due to the fact that for $\mu > \mu_{c2}$, the LPT trajectory connects the two distinct localized states i.e. $\theta = 0$ (energy localization on the first oscillator) with $\theta = \pi/2$ (energy localization on the second oscillator) interval $(0, \pi/2)$; in turn, by the polar transformations Eq. (2.36) we deduce that intense energy exchanges between the two oscillators take place on the LPT (and on quasi-periodic orbits in its vicinity), with energy being continuously exchanged between the first oscillator (where the energy is localized for $\theta \approx 0$) and the second (for $\theta \approx \pi/2$). At $\mu = \mu_{c2}$ the LPT coincides with the speratrix emanating form the unstable out-of-phase NNM, signifying the end of strong energy exchanges in the dynamics. Indeed, for $\mu < \mu_{c2}$, the topological structure of the LPT changes from a single spatially extended orbit to two spatially localized orbits, with drastically decreased ranges in terms of θ for each orbit. This indicates a transition of the resonant non-stationary dynamics of the system, since for $\mu < \mu_{c2}$, the oscillations of system (2.28) become localized to either one of the two oscillators (within each of the two disjoint LPTs) and the intensity of energy exchanges between oscillators drastically decreases. Further decrease in μ enhances the intensity of energy

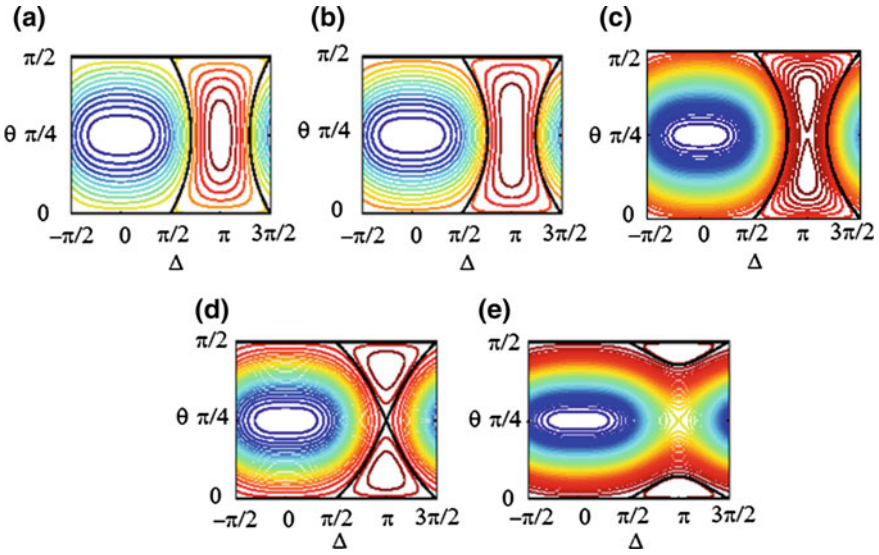

Fig. 2.12 Reduced slow flow on the isoenergetic two-torus (2.38a and 2.38b) for **a** $\mu = 1.4$, **b** $\mu = \mu_{c1} = 1.0$, **c** $\mu = 0.8$, **d** $\mu = \mu_{c2} = 0.6$, **e** $\mu = 0.3$; the LPTs are indicated by the bold lines. Different colors in contour lines correspond to values of the integral (2.39) and are used to highlight the topology of the dynamics on the torus

localization in either one of the two oscillators and energy exchanges between them increasingly diminish.

The change of the topological structure of the LPT for varying μ is numerically shown in Fig. 2.13, where the two LPTs on the two-torus (Eqs. 2.38a and 2.38b) for initial conditions $\theta(0) = 1 \times 10^{-3}$ and $\Delta(0) = 0$ (corresponding to energy initially localized to the first oscillator), and values of μ before and after the LPT bifurcation are depicted. We note that in the regime of strong energy exchanges $(\mu = 0.8 > \mu_{c2})$, the dependencies of the angles θ and Δ on the rescaled slow time $\bar{t}_1$ for the LPT are non-smooth, resembling sawtooth, and square-wave functions, respectively; whereas in the regime of localization $(\mu = 0.3 < \mu_{c2})$ the angles for the LPT have smoother waveforms. These observations will help us derive analytical approximations for these orbits representing non-stationary dynamics in the next section. In Fig. 2.14, we confirm the previous analytical predictions by direct numerical simulations of system (9) with initial conditions $v_1(0) = 1$ and $v_1'(0) = v_2(0) = v_2'(0) = 0$ and varying values of μ before and after the LPT bifurcation. The predicted strong resonant energy exchanges before the bifurcation and the localization of the motion after it are numerically verified from these results.

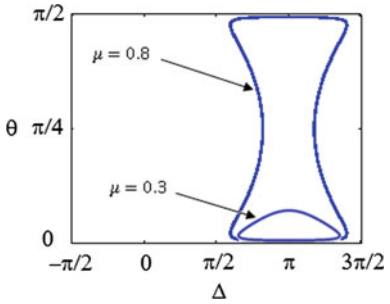

Fig. 2.13 Topological change of the LPT before and after the second bifurcation point $\mu = \mu_{c2} = 0.6$ and initial energy localized to the first oscillator: **a** $\mu = 0.8$ corresponding to strong energy exchanges between the two oscillators and spatially extended LPT on the two-torus, **b** $\mu = 0.3$ corresponding to localization in the first oscillator and spatially localized LPT

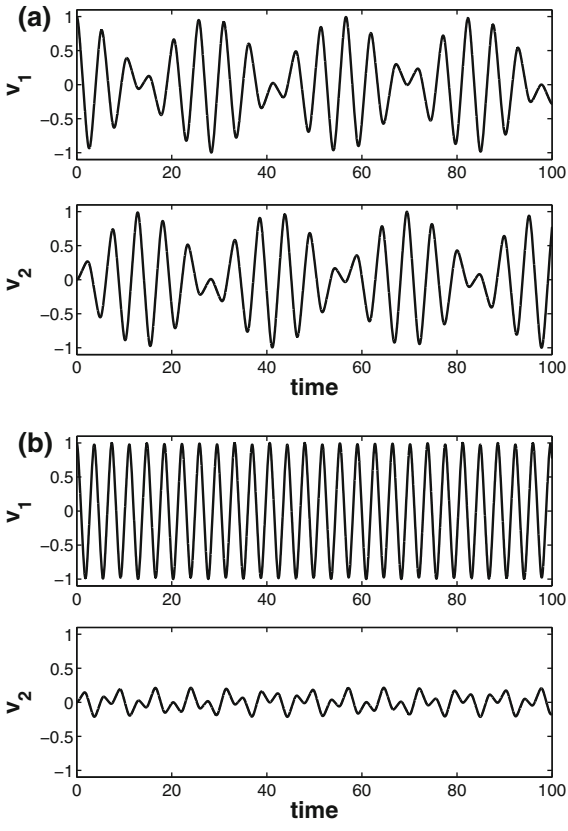

Fig. 2.14 Direct numerical simulations of system (2.28) for the case when initial energy is confined in the first oscillator ($v_1(0) = 1$ and $v_1'(0) = v_2(0) = v_2'(0) = 0$) and **a** $\mu = 0.8$, **b** $\mu = 0.3$

2.2.5 Analytical Approximations of the LPTs on the Two-Torus

The numerical results of the previous section highlight the importance of the LPT for understanding of resonant energy exchanges between the two coupled oscillators in system (2.28). Hence, in this section, we provide an analytical study of the LPTs in the regimes before and after their bifurcation with the separatrix on the two-torus. First, we start with the analysis of the LPT for $\mu > \mu_{c2}$, in the regime where intense energy exchanges between the two oscillators Eq. (2.28) take place. This analysis is motivated by the numerical results depicted in Fig. 2.13a which provide insight on the highly non-stationary dynamics on the two-torus Eqs. (2.38a) and (2.38b) corresponding to the LPT.

To this end, we reconsider the reduced slow flow Eqs. (2.38a) and (2.38b) in the regime before the second bifurcation and develop analytical approximations for the LPT by noting that on that orbit the dependencies of the angles θ and Δ with respect to the rescaled slow timescale $\bar{t}_1$ are periodic but discontinuous, resembling sawtooth and square-wave functions, respectively (see Fig. 2.13a). At this point, we need to emphasize that an LPT is a period orbit in the slow torus with *finite period*, contrary to a separatrix in the same torus which is an orbit of *infinite period*. Motivated by these observations, we resort to the method of non-smooth temporal transformations (Pilipchuk 2010) for analytically studying periodic orbits (and their bifurcations) of strongly nonlinear dynamical systems. We express the sought LPTs in terms of two new non-smooth variables, τ and e, as follows,

$$\begin{aligned} \theta(\bar{t}_1) &= X_1[\tau(\bar{t}_1/a)] + e(\bar{t}_1/a)Y_1[\tau(\bar{t}_1/a)] \\ \Delta(\bar{t}_1) &= X_2[\tau(\bar{t}_1/a)] + e(\bar{t}_1/a)Y_2[\tau(\bar{t}_1/a)] \end{aligned} \tag{2.40}$$

where $a = T/4$ represents the (yet unknown) quarter-period of the LPT in terms of the rescaled slow timescale $\bar{t}_1$. The non-smooth functions τ and e are used to replace the slow timescale $\bar{t}_1$ in the reduced system (2.38a) and (2.38b) and are defined by the expressions,

$$\tau(x) = \frac{1}{2}\left(\frac{2}{\pi}\sin^{-1}\left(\sin\left(\pi x - \frac{\pi}{2}\right) + 1\right)\right), \quad e(x) = \frac{\mathrm{d}\tau(x)}{\mathrm{d}x} \tag{2.41}$$

The representations (2.4) provide decompositions of a periodic functions $\theta(\tilde{t}_1)$ and $\Delta(\tilde{t}_1)$ in terms of symmetric (the X-components) and anti-symmetric (the Y-components) parts. Moreover, considering the numerical time series of these angles for the LPT of Fig. 2.13a, we need to set $Y_1[\tau(\tilde{t}_1/a)] = X_2[\tau(\tilde{t}_1/a)] = 0$ in Eq. (2.40) so that the analytical representations for the angles $\theta(\tilde{t}_1)$ and $\Delta(\tilde{t}_1)$ resemble sawtooth and a square-wave waveforms, respectively, and retain the symmetric and anti-symmetric features, respectively, of the numerical results. In the following analysis, we consider only the leading-order approximations for the

functions X_1 and Y_2, and of the quarter-period a; for a regular perturbation scheme for estimating higher-order approximations, we refer to (Manevitch and Smirnov 2010c: 3).

Considering the first integral (2.39) of the reduced slow flow, and imposing the condition that the LPT passes through the point $(\theta, \Delta) = (0, 0)$, we compute $H = 3/4$, so the equation describing the LPT on the two-torus is given by,

$$\mu\left(\frac{1}{2}\,\sin^2 2\theta\,\cos 2\Delta - 2\,\sin 2\theta\,\cos\Delta\right) + \frac{3}{4}\,\cos 4\theta = \frac{3}{4} \tag{2.42a}$$

leading to the following functional relationship between the angles θ and Δ:

$$\cos\Delta = \frac{1}{\sin 2\theta} \pm \sqrt{\frac{1}{\sin^2 2\theta} + \frac{\mu+3}{2\mu}} \tag{2.42b}$$

In the following analysis, we consider only the $(-)$ sign in this expression so the result holds for $0 < \bar{t}_1 < a$, i.e., over a quarter-period of the LPT [in fact, this result estimates the component $Y_2[\tau(\bar{t}_1/a)]$ in (2.40)]. Over the same quarter-period, the angle θ varies linearly in $\bar{t}_1$ between the two limiting values 0 and $\pi/2$, corresponding to energy confined in the first and the second oscillator, respectively, (this estimates the component $X_1[\tau(\bar{t}_1/a)]$ in Eq. (2.40). To extend these analytical results over the entire time domain and obtain a symmetric periodic representation for the angle $\theta(\bar{t}_1)$, and an anti-symmetric representation for the angle $\Delta(\bar{t}_1)$, we take into account Eq. (2.40) and express the leading-order analytical approximation for the LPT as:

$$\begin{aligned} \theta(\bar{t}_1) &= \tfrac{\pi}{2}\tau\left(\tfrac{\bar{t}_1}{a}\right) \\ \Delta(\bar{t}_1) &= -e\left(\tfrac{\bar{t}_1}{a}\right)\,\cos^{-1}\left[\frac{-\frac{\mu+3}{2\mu}\,\sin\left(\pi\tau\left(\frac{\bar{t}_1}{a}\right)\right)}{1+\sqrt{1+\frac{\mu+3}{2\mu}\,\sin^2\left(\pi\tau\left(\frac{\bar{t}_1}{a}\right)\right)}}\right] \end{aligned} \tag{2.43}$$

Note that by the definitions of the non-smooth variables Eq. (2.41), we get a symmetric (odd) sawtooth-like periodic extension for $\theta(\bar{t}_1)$, and an anti-symmetric (even) square-wave-like periodic extension for $\Delta(\bar{t}_1)$. These results are in full agreement with the numerical waveforms depicted in Fig. 2.14.

Now, it remains to analytically estimate the period $T = 2a$ of the LPT. This can be performed in terms of a definite integral, since Eq. (2.42b) yields the dependence $\Delta = \Delta(\theta)$. In addition, from Eq. (2.38a), we can write that

$$\mathrm{d}\bar{t}_1 = \frac{\mathrm{d}\theta}{2(\sin 2\theta\,\sin 2\Delta - 2\,\sin\Delta)} \;\Rightarrow\; \int_0^a \mathrm{d}\bar{t}_1 = \int_0^{\pi/2} \frac{\mathrm{d}\theta}{2(\sin 2\theta\,\sin 2\Delta - 2\,\sin\Delta)} \tag{2.44a}$$

or

$$a = \int_0^{\pi/2} \frac{\mathrm{d}\theta}{2(\sin 2\theta \ \sin 2\Delta(\theta) - 2 \ \sin \Delta(\theta))} \tag{2.44b}$$

This is the exact expression for the half-period of the LPT in slow time and yields excellent agreement with the results of direct numerical integration of system (2.20) (cf. Fig. 2.15). This last computation completes the leading-order analytical approximation for the LPT before the second bifurcation (i.e., in the regime of intense energy exchanges between the oscillators), given by Eq. (2.43) and (2.44b). The derived analytical approximations can be used for analytically studying the strongly nonlinear, non-stationary dynamics of system Eq. (2.28) involving highly intense energy exchanges between the two oscillators.

Considering the original system Eq. (2.28) governing the transverse oscillations of the two particles, assuming initial conditions $v_1(0) = 1$ and $v_1'(0) = v_2(0) = v_2'(0) = 0$, and that $\delta_1 = 0, \delta_2 = \Delta$, the leading-order approximation for the LPT in the highly intense energy exchange of the dynamics is expressed as $v_1(\tilde{t}) \approx \cos(\theta(\tilde{t}/32\omega)) \ \sin(\omega\tilde{t})$ and $v_2(\tilde{t}) \approx \sin(\theta(\tilde{t}/32\omega)) \ \sin(\omega\tilde{t} + \Delta(\tilde{t}/32\omega))$. In Fig. 2.15, we compare the analytical approximations with the numerical solutions for the LPT corresponding to $\mu = 0.8$ (cf. Fig. 2.13a) and the aforementioned initial conditions, and note satisfactory agreement.

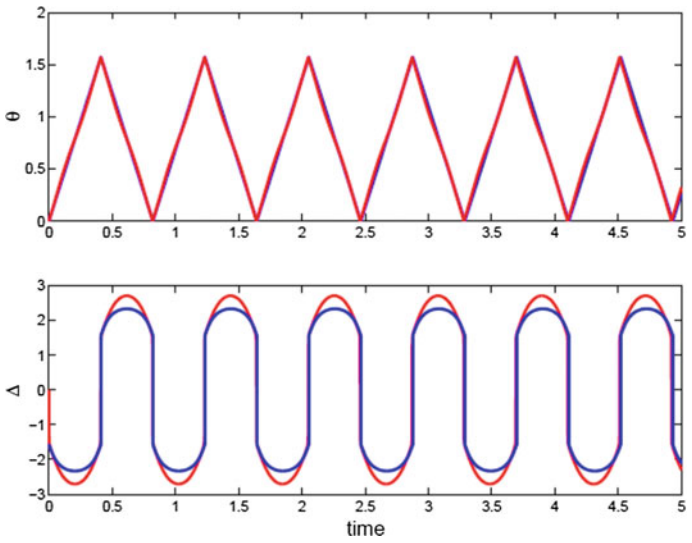

Fig. 2.15 Comparison between the analytical solution for the LPT derived by Eqs. (2.43) and (2.44b) (*blue* (*solid*) *line*), and the LPT computed by direct numerical simulation of Eq. (2.28) (*red* (*solid*) *line*) for $\mu = 0.8$ (regime of intense energy exchanges between the oscillators)

We now analyze the LPT for $\mu < \mu_{c2}$, i.e., in the regime where weak energy exchanges between the two oscillators Eq. (2.28) take place, and the oscillations are localized in either one of them. This analysis is motivated by the numerical results depicted in Fig. 2.13b which provide insight on the near-stationary dynamics on the two-torus (2.38a) and (2.38b) corresponding to the LPT in that regime of the dynamics. We note that although we employ to term "localization," to describe the transverse oscillations of system (2.28) and the absence of *complete* energy exchange, the two particles' *partial* energy exchange is still possible. In this case, the LPT corresponds to the orbit where maximum possible (partial) energy exchange between the two oscillators (2.28) occurs. Moreover, in contrast to the previous regime of intense resonant energy exchange, for $\mu < \mu_{c2}$, there are two disjoint LPTs corresponding to localized resonant oscillators to either one of the two oscillators.

Similar to the previous case of full energy exchange, the LPT is defined as the trajectory which passes through the point $(\theta, \Delta) = (0, 0)$. Hence, all previous calculations still hold and the functional relation between the angle variables on the LPT can be expressed as Eq. (2.42b). In turn, the temporal dependencies of the two angle variables are expressed as

$$\begin{aligned} \theta(\tilde{t}_1) &= A\ \tau\left(\frac{\tilde{t}_1}{a}\right) \\ \Delta(\tilde{t}_1) &= e\left(\frac{\tilde{t}_1}{a}\right)\left\{\pi - \cos^{-1}\left[\frac{1}{\sin\left(2A\ \tau\left(\frac{\tilde{t}_1}{a}\right)\right)} \pm \sqrt{\frac{1}{\sin^2\left(2A\ \tau\left(\frac{\tilde{t}_1}{a}\right)\right)} + \frac{\mu+3}{2\mu}}\right]\right\} \end{aligned} \tag{2.45a}$$

where the amplitude A is determined from the energy-conservation first integral (2.39) as

$$A = \frac{1}{2}\sin^{-1}\left(\frac{4-\mu}{3\mu}\right) \tag{2.45b}$$

and the period $T = 2a$ by employing the methodology outlined for the LPT in the regime of intense energy exchanges:

$$a = \int_0^A \frac{\mathrm{d}\theta}{2(\sin 2\theta\ \sin 2\Delta(\theta) - 2\ \sin \Delta(\theta))} \tag{2.45c}$$

As shown in Fig. 2.16, the comparison between the analytical solutions (2.45a), (2.45b) and direct numerical simulations of the original system (2.28) is satisfactory.

This completes the analytical and numerical study of the transverse oscillations of system (2.28), including both the stationary and non-stationary regimes and bifurcations of these motions. In the next section, we consider the axial motions of the system of two particles governed by the singularly perturbed Eqs. (2.24a)

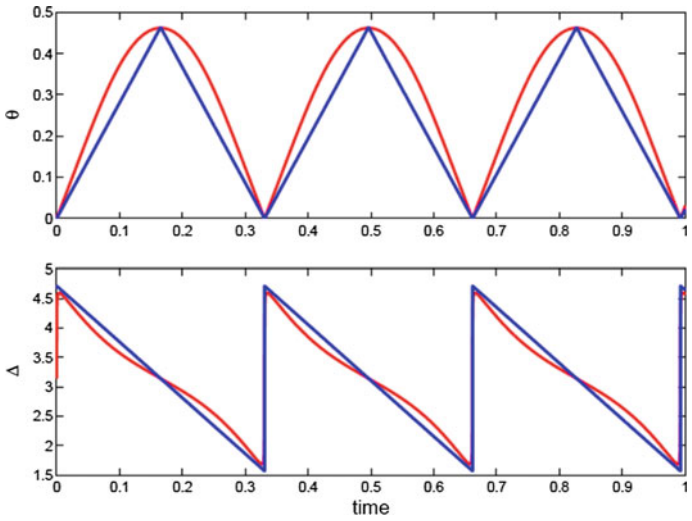

Fig. 2.16 Comparison between the analytical solution for the LPT derived by (2.45a)–(2.45c) (*blue* (*solid*) *line*), and the LPT computed by direct numerical simulation of (2.28) (*red* (*solid*) *line*) for $\mu = 0.3$ (regime of weak energy exchanges between the oscillators)

2.2.6 *Mixed Slow/Fast Axial Oscillations for n = 2*

To obtain the leading-order analytical approximations for the axial oscillations of the particles, we reconsider system (2.24a) which for $n = 2$ is expressed as:

$$\begin{aligned} \varepsilon^2 u_1'' + (2u_1 - u_2) &= -\tfrac{1}{2}\left[v_1^2 - (v_2 - v_1)^2\right] + \cdots \\ \varepsilon^2 u_2'' + (2u_2 - u_1) &= -\tfrac{1}{2}\left[(v_2 - v_1)^2 - v_2^2\right] + \cdots \end{aligned} \tag{2.46}$$

This problem can be solved by noting that having already computed the analytical approximations for the transverse displacements v_i, the dynamical system (2.46) can be regarded as a system of two coupled *linear* oscillators forced by "pseudo-forcing" terms on the right-hand sides, and so can be studied by standard linear modal analysis. Then, the leading-order approximations of the amplitudes of the axial oscillations contain both *slow* (represented by the particular solutions) and *fast* (resulting from the homogeneous solutions) components. We have seen that the slow dynamics is critical for realizing the nonlinear acoustic vacuum in terms of transverse oscillations (providing the approximately uniform, in the slow scale, axial tension in the system), and play the main role in constructing the leading-order approximations. Regarding the axial oscillations of the particles, however, in addition to the slow dynamics, the fast dynamics need also to be explicitly taken into account in the leading-order approximation in order to satisfy the initial conditions for the axial oscillations of the problem (this is demonstrated in the

following example for in-phase transverse oscillations). The combined effect of this mixed slow/fast dynamics is a fast redistribution of axial forces from an arbitrary initial state to a nearly uniform state in slow time which is necessary for the realization of the nonlinear sonic vacuum.

We demonstrate this computation by considering the in-phase mode for transverse oscillations, but a similar procedure can be followed for the other NNMs or for non-stationary resonant motions such as the LPTs. Accordingly, we set $v_1 = v_2 \equiv v$ and introduce the modal coordinates $\xi_1 = u_1 + u_2$ and $\xi_2 = u_2 - u_2$ to express Eq. (2.46) as:

$$\begin{aligned} \varepsilon^2 \xi_1'' + \xi_1 &= 0 + \cdots \\ \varepsilon^2 \xi_2'' + 3\xi_2 &= -v^2 + \cdots \end{aligned} \tag{2.47}$$

where the transverse displacement $v(\tilde{t})$ is computed by solving for the nonlinear modal oscillator (2.29b) with $k = 1$

$$v'' + [(1/3) + (1/\mu)]v^3 = 0 \Rightarrow v(\tilde{t}) = V \,\mathrm{cn}\left(\sqrt{L}\tilde{t}, 1/\sqrt{2}\right) \tag{2.48}$$

where $L = (1/3) + (1/\mu)$, $cn(\cdot,\cdot)$ is the Jacobi elliptic cosine function, and the initial conditions for the transverse oscillations are assumed in the form $v(0) = V, v'(0) = 0$. Substituting (2.48) into (2.47), solving the resulting nonhomogeneous system, and transforming back to original coordinates, we derive the following leading-order approximations for the axial displacements

$$\begin{aligned} u_1(\tilde{t}) &= \underbrace{C_1 \cos(\tilde{t}/\varepsilon) + C_2 \sin(\tilde{t}/\varepsilon) + C_3 \cos\left(\tilde{t}\sqrt{3}/\varepsilon\right) + C_4 \sin\left(\tilde{t}\sqrt{3}/\varepsilon\right)}_{\text{Fast oscillations}} + \underbrace{v^2/6}_{\text{Slow oscillations}} + \cdots \\ u_2(\tilde{t}) &= \underbrace{C_1 \cos(\tilde{t}/\varepsilon) + C_2 \sin(\tilde{t}/\varepsilon) - C_3 \cos\left(\tilde{t}\sqrt{3}/\varepsilon\right) - C_4 \sin\left(\tilde{t}\sqrt{3}/\varepsilon\right)}_{\text{Fast oscillations}} - \underbrace{v^2/6}_{\text{Slow oscillations}} + \cdots \end{aligned} \tag{2.49}$$

where the coefficients of the fast oscillations are determined by imposing the initial conditions for the axial oscillations, and we recall the rescaling of the time variable introduced in Sect. 2.2, $\tilde{t} = \varepsilon(k_1/m)^{1/2}t$, in terms of the physical time t. Note that apart from the mixed slow/fast dynamics, the axial dynamics also mix the in-phase and out-of-phase axial modes at the fast timescale of the problem.

As discussed above and confirmed by (2.49), the leading-order approximations for the axial oscillations consist of two parts, namely of fast oscillations with two different fast frequencies, and of slow oscillations which have the same frequency as the leading-order (slow) approximations of the transversal oscillations. These fast axial oscillations play an important role in the dynamics since the generate the non-local effects in the transverse dynamics by providing the fast redistribution of

axial forces from an arbitrary initial distribution to a nearly uniform state in the slow timescale which ultimately generates the nonlinear sonic vacuum.

To demonstrate the validity of the asymptotic analysis, in Fig. 2.17, we depict the direct numerical integration of the equations of motion of the original system (2.24a), (2.24b) for $n = 2$, for the case of the LPT in the regime of intense energy exchange (after the first but before the second bifurcation), and compare them with the leading-order analytical results derived by the slow/fast decompositions. Satisfactory agreement between the asymptotic and numerical results is noted, confirming the validity of our theoretical predictions.

2.2.7 Global Dynamics

Since contrary to the reduced slow flow on the two-torus Eqs. (2.38a), (2.38b), system (2.28) is not integrable (since it possesses only one first integral of motion corresponding to energy conservation), we performed an additional study to clarify its global dynamics and confirm the theoretical predictions of the previous section which were based on asymptotic analysis of the slow dynamics. This analysis was based on the construction of numerical Poincaré maps and clarified the role of the resonance dynamics and of NNM and LPT bifurcations on the non-stationary and chaotic dynamics of the strongly nonlinear system (2.28).

To this end, we consider the four-dimensional phase space $\left(v_1, v_2, v_1', v_2'\right) \in R^4$ of system (2.28) and reduce the dynamics to a three-dimensional isoenergetic manifold by fixing the total energy (hamiltonian) of this system to a constant value $F\left(v_1, v_2, v_1', v_2'\right) = f \Rightarrow v_2' = F^{-1}\left(v_1, v_2, v_1'; f\right)$. This renders $\dot{v}_2$ a dependent variable. Then, we introduce the Poincaré cut section $\Sigma = \left\{\left(v_1, v_2, v_1', F^{-1}\left(v_1, v_2, v_1'; f\right)\right) \in R^3 / v_2 = 0, v_2' > 0\right\} \cap F\left(v_1, v_2, v_1', v_2'\right) = f$ and define the Poincaré map,

$$P : \Sigma \to \Sigma : \left\{\left(v_1(t_k), v_1'(t_k)\right) \to \left(v_1(t_{k+1}), v_1'(t_{k+1})\right)\right\}$$

where t_k and t_{k+1} denote consecutive time instances of crossings of orbits on the isoenergetic manifold with the cut section Σ. By this construction, the Poincaré is orientation preserving and captures all the global dynamics on the cut section (since it can be proven that the isoenergetic flow is always transversal to Σ, with the only exception being at the boundary of the map where $v_2' = 0$).

In the following numerical results, we fix the hamiltonian of system (2.28) to $F = 10$, and consider the global dynamics for varying values of μ; moreover, we denote the LPTs on the Poincaré maps by bold lines. In Fig. 2.18, we depict the Poincaré maps of (2.28) for $\mu = 1.6, 0.8$ and 0.3, and the global numerical analysis fully confirms and validates our asymptotic results. The NNMs of the system are fixed points of the map on the horizontal axis $v_1' = 0$ and the bifurcation of these stationary solutions at the first bifurcation point $\mu_{c1} = 1$ can be clearly observed in

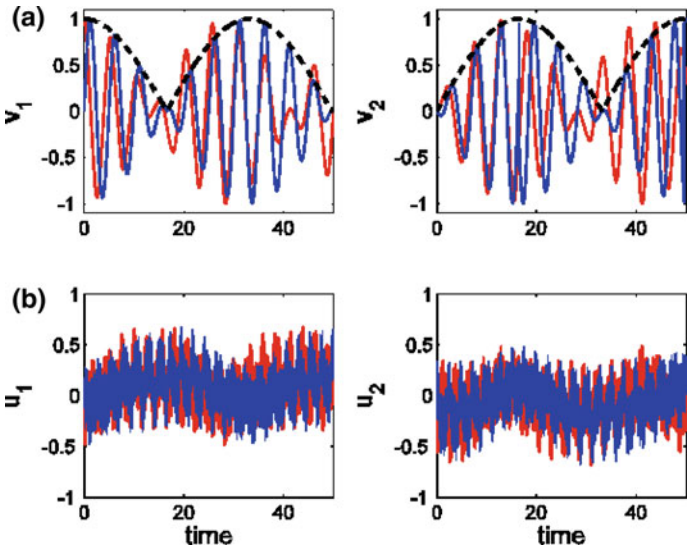

Fig. 2.17 Comparison between theoretical prediction and numerical simulation for the LPT of the system with $n = 2$, $\mu = 0.8, \varepsilon = 0.05$ and initial conditions $v_1(0) = 1$, $v_1'(0) = v_2(0) = v_2'(0) = 0$, and $u_1(0) = u_1'(0) = u_2(0) = u_2'(0) = 0$: **a** Transverse displacement $v_1(t)$, and **b** axial displacement $u_1(t)$; the asymptotic predictions (2.43, 2.44a, 2.44b and 2.46 are denoted by *blue solid*) lines, while the numerical simulations of Eqs. (2.24a), (2.24b) by *red* (*solid*) *lines*; the *bold dashed line* in (**a**) shows the analytical prediction of the (slow) envelope

the numerical results. Moreover, the stability of the two NNMs before the bifurcation (with the NNMs are depicted as centers—cf. Fig. 2.18a) and the instability of the out-of-phase NNM after the bifurcation (with the mode depicted as a saddle point—cf. Fig. 2.18b) are clearly inferred. In addition, the change of the topological structure of the LPT from spatially extended to spatially localized after the second bifurcation point $\mu_{c2} = 0.6$ is also confirmed. In particular, in Fig. 2.17c, we note the result of the LPT bifurcation, which is signified by the existence of two disjoint LPTs, with each of them being localized in the neighborhood of either one of the stable bifurcated NNMs.

Additionally, we note that the region of chaotic motions depends strongly on the value of parameter μ. When μ is large enough (far from both topological transformations resulting from the two bifurcations of the global dynamics), the regions of chaos are nearly negligible (cf. Fig. 2.18a), and the entire phase space of the system seems to be foliated by isoenergetic invariant tori where the global dynamics are topologically similar to the reduced slow flow two-torus (2.38a and 2.38b); given, however, that the dynamical system (2.28) is non-integrable, we infer that even in this case chaotic layers still exist by they are spatially confined. Hence, in this case, the asymptotic analysis based on slow flow reduction fully reflects the behavior of the non-integrable system (2.28).

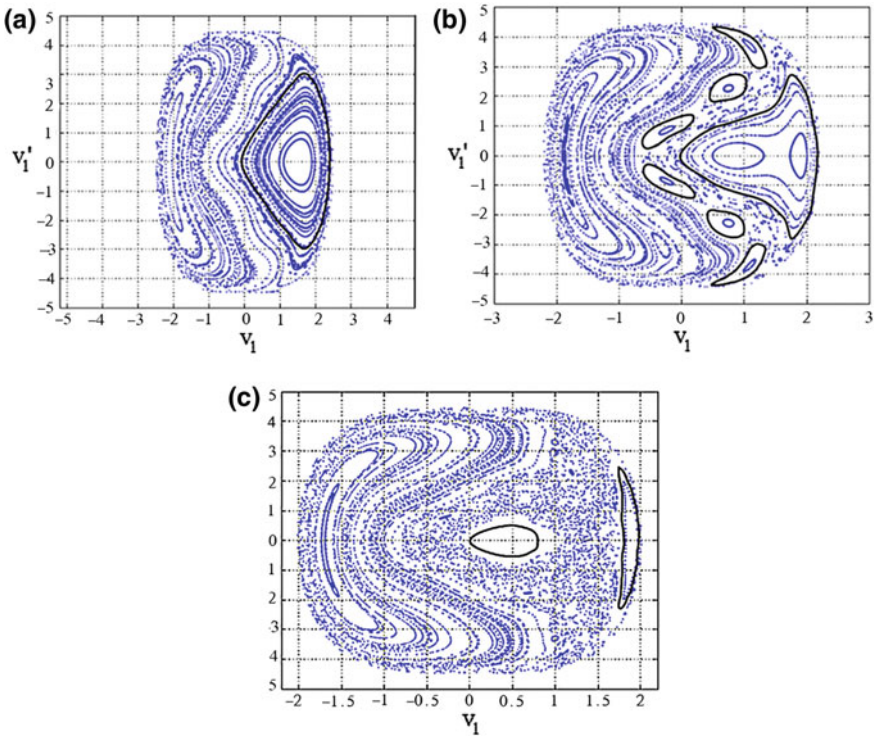

Fig. 2.18 Poincaré maps depicting the global dynamics of system (2.28) for **a** $\mu = 1.6$, **b** $\mu = 0.8$, and **c** $\mu = 0.5$; LPTs are denoted by *bold lines*

After the first topological transition (cf. Fig. 2.18b), a weak chaotic layer appears, together with a set of secondary stationary points. These points correspond to periodic motions satisfying conditions of 1:3 internal resonance so they are not captured by our previous asymptotic analysis which is based on the assumption of 1:1 resonance. This higher-order resonance dynamics can be also treated analytically, e.g., with the methodologies developed in (2.32 and 2.33). The 1:3 resonant stationary points are surrounded by secondary LPTs which correspond to less intense energy exchanges between the two oscillators in Eq. (2.28). Finally, after the second transition takes place (cf. Fig. 2.18c), the chaotic region expands, and the regime of regular dynamics is confined only in the neighborhoods of the bifurcated NNMs where the two bifurcated localized LPTs can be seen. In this case, the two LPTs provide the boundaries between the regimes of chaotic and regular dynamics.

Thus, the presence of strongly nonlinear elastic supports changes qualitatively both the stationary and non-stationary resonance dynamics of the nonlinear sonic vacuum. Considering the simplest case of the system with only two particles, we showed that, in contrast to the ungrounded sonic vacuum studied, there occur two main bifurcations (dynamical transitions) in the dynamics under condition of 1:1

resonance. First, a bifurcation of NNMs generates a pair of localized bifurcating NNMs and an unstable out-of-phase NNM; such NNMs bifurcations are not possible in the ungrounded sonic vacuum whose NNMs are identical to those of the corresponding linear spring-mass chain. Second, a bifurcation of the LPT which changes drastically the intensity of energy exchanges occurring between the two oscillators of the system; again this type of LPT bifurcation is not possible in the ungrounded sonic vacuum where, under certain conditions, only a single LPT can occur corresponding to intense energy exchanges between different NNMs in 1:1 resonance.

The analytical and numerical results presented here show that, alongside with well-known bifurcation and instability of NNMs (Manevitch and Smirnov 2010c: 3), full energy exchanges between different parts of the sonic vacuum become possible in the regime of spatially extended LPTs. For different values of the system parameters and depending on the energy level of the oscillation, the LPTs can become localized in neighborhoods of bifurcated NNMs, in which case the intensity of energy exchanges in the resonant non-stationary dynamics of the sonic vacuum drastically decreases. This type of strongly non-stationary phenomena can be adequately described by LPTs whose analytical presentation was obtained in terms of non-smooth basic functions. An asymptotic analysis performed under condition of 1:1 resonance and based on slow/fast decomposition of the dynamics fully predicted these previous global dynamical changes. Moreover, it was shown that chaotic effects due to the non-integrable nature of the sonic vacuum could not affect the bifurcations and the corresponding topological changes in the phase space predicted by the slow flow asymptotic analysis. Another interesting finding was that the LPTs appeared to separate the regions of regular dynamics in-phase space from the surrounding local or global chaotic layers.

The results presented in this section can be extended to sonic vacua with larger number of particles, but the analysis of these higher-dimensional systems is much more complex (we present such analysis in Part 3). In addition, a new family of sonic vacua composed of a number of parallel coupled chains of particles similar to the one shown in Fig. 2.11 can be constructed and its stationary and non-stationary resonant dynamics examined. Then, it would be of interest to examine the NNMs, LPTs, and their bifurcations of this class of essentially nonlinear "discrete membranes." Finally, from a practical viewpoint, it is significant that the number of resonating modes in the discrete model of untensioned grounded string may exceed that of the corresponding ungrounded system and that the non-stationary dynamics and nature of resonant energy exchanges and LPTs in these two systems are completely different.

Let us note that the obtained results for the two-particle modes are similar to those presented in the previous section in the case of cubic nonlinearity. Despite the parameters determining a qualitative change of non-stationary and non-stationary dynamics are different, the types of dynamical behavior turn out to be similar (excluding the longitudinal motion which is absent in the case of local sonic vacuum).

References

Manevitch, L.I.: Complex representation of dynamics of coupled nonlinear oscillators, In: Uvarova, L., Arinstein, A.E., Latyshev, A.V. (eds.), Mathematical Models of Non-Linear Excitations. Transfer, Dynamics, and Control in Condensed Systems and Other Media, pp. 269–300. Springer, New York (1999)

Manevitch, L.I.: The description of localized normal modes in a chain of nonlinear coupled oscillators using complex variables. Nonlinear Dyn. **25**, 95 (2001)

Manevitch, L.I.: New approach to beating phenomenon in coupled nonlinear oscillatory chains. In: Awrejcewicz, J., Olejnik, P. (ed.) 8th Conference on Dynamical Systems-Theory and Applications (DSTA-2005), p. 289 (2005)

Manevitch, L.I.: New approach to beating phenomenon in coupled nonlinear oscillatory chains. Arch. Appl. Mech. **301** (2007)

Manevitch, L.I., Gendelman, O.V.: Tractable Models of Solid Mechanics. Springer, Berlin (2011)

Manevitch, L.I., Musienko, A.I.: Limiting phase trajectories and energy exchange between an anharmonic oscillator and external force. Nonlinear Dyn. **58**, 633–642 (2009)

Manevitch, L.I., Smirnov, V.V.: Localized nonlinear excitations and interchain energy exchange in the case of weak coupling. In: Awrejcewicz, Jan (ed.) Modeling, Simulation and Control of Nonlinear Engineering Dynamical System, pp. 37–47. Springer, Netherlands (2009)

Manevich, L.I., Smirnov, V.V.: Limiting phase trajectories and thermodynamics of molecular chains. Phys. Doklady **55**, 324–328 (2010)

Manevitch, L.I., Smirnov, V.V.: Limiting phase trajectories and the origin of energy localization in nonlinear oscillatory chains. Phys. Rev. E **82** (2010b)

Manevitch, L.I., Smirnov, V.V.: Resonant energy exchange in nonlinear oscillatory chains and limiting phase trajectories: from small to large systems. In: Vakakis, A.F. (ed.) Advanced Nonlinear Strategies for Vibration Mitigation and System Identification, CISM Courses and Lectures, 518, pp. 207–258. Springer, New York (2010c)

Manevitch, L.I., Vakakis, A.F.: Nonlinear oscillatory acoustic vacuum. SIAM J. Appl. Math. **74** (6), 1742–1762 (2014)

Pilipchuk, V.N.: Nonlinear Dynamics: Between Linear and Impact Limits. Springer, Berlin (2010)

Starosvetsky, Y., Ben-Meir, Y.: Nonstationary regimes of homogeneous Hamiltonian systems in the state of sonic vacuum. Phys. Rev. E **87**, 062919 (1–18) (2013)

Vakakis, A.F., Manevitch, L.I., Mikhlin, YuV, Pilipchuk, V.N., Zevin, A.A.: Normal Modes and Localization in Nonlinear Systems. Wiley, New York (1996)

Zhupiev, A.L., Mikhlin, Y.V.: Stability and branching of normal oscillation forms of non-linear systems. J. Appl. Math. Mech. **45**, 328–331 (1981)

Zhupiev, A.L., Mikhlin, Y.V.: Conditions for finiteness of the number of instability zones in the problem of normal vibrations of non-linear systems. J. Appl. Math. Mech. **486–489**, 48 (1984)

http://www.springer.com/978-981-10-4665-0

Nonstationary Resonant Dynamics of Oscillatory Chains and Nanostructures

Manevitch, L.I.; Kovaleva, A.; Smirnov, V.; Starosvetsky, Y.

2018, XXII, 436 p. 194 illus., 116 illus. in color.,
Hardcover
ISBN: 978-981-10-4665-0